ABSTRACT

MCKAY, TRAVIS JOSHUA. Quartz Crystal Microbalance Biosensor Toward Next-Generation Detection of Physiologically Relevant Analytes. (Under the direction of Dr. Michael Daniele).

Alternative and novel detection methods utilizing biosensors have always been studied for their diagnostic potential and minimal invasiveness. The development of a quartz crystal microbalance (QCM) biosensor is described for its capacity toward next-generation biosensing applications, namely, biosensor regeneration and arrayed detection. Herein, the design and construction of the surface chemistry and custom biosensor are discussed as well as the initial evaluation of system performance for capturing immunoglobulin G (IgG) analyte. The surface chemistry was based on the principles of self-assembled monolayers (SAM), immobilizing the HWRGWV peptide on the gold electrode surface to bind IgG. Surface characterization was carried out using ellipsometry, fluorescence microscopy, atomic force microscopy (AFM), and surface plasmon resonance (SPR). These techniques highlighted the structure and successful functionalization of the biosensor surface. The QCM demonstrated the ability to detect concentrations of IgG across a dynamic range of 10 μg/mL to 1 mg/mL, with a resonant frequency shift on the order of 30-100 Hz at saturation. Next-generation applications for the basis of future work were explored through biosensor regeneration studies including the use of sodium phosphate buffer in NaCl, and via the design of a 4-channel arrayed QCM biosensor.

Quartz Crystal Microbalance Biosensor Toward Next-Generation Detection of Physiologically Relevant Analytes

by
Travis Joshua McKay

A thesis submitted to the Graduate Faculty of
North Carolina State University
in partial fulfillment of the
requirements for the degree of
Master of Science

Biomedical Engineering

Raleigh, North Carolina
2024

APPROVED BY:

_____	_____
Dr. Michael Daniele Committee Chair	Dr. Koji Sode
_____	
Dr. Kennita Johnson	

DEDICATION

To my cherished family and beloved friends.

BIOGRAPHY

Travis Joshua McKay was born in Brooklyn, New York on June 12, 1996. Upon moving to North Carolina in 2008, he continued to develop a passion for learning as well as the deliciousness of buttermilk biscuits. Travis attended high school at the North Carolina School of Science and Mathematics then earned his B.S. in Chemical Engineering at the University of Maryland, Baltimore County before pursuing graduate studies in Biomedical Engineering back home at North Carolina State University. He hopes to combine his engineering background and entrepreneurial mindset to leave a mark on the world and the lives of others.

ACKNOWLEDGMENTS

Thank you to my family and friends for always being there throughout the highs and lows of graduate school, as well as the members of the BioInterface Lab for making Centennial Campus a fun and intellectually stimulating place to work. Thanks to Dr. Mike Wilkins for giving me a soft landing into the world of electronics. Special thanks to Junhyeong Wang, Dr. BangHyun Lee, and Dr. Srivatsan Ramesh for their collaboration and support on the QCM project. An extra special thanks to Dr. Joel Ducoste for influencing my decision to return to graduate school and obtain my M.S. degree. Lastly, I would like to thank Dr. Michael Daniele for fostering a research environment that enables people to grow scientifically and personally toward their goals.

TABLE OF CONTENTS

LIST OF FIGURES

1. INTRODUCTION

The biosensor has emerged as a promising tool for the prevention and monitoring of diseases since its inception in 1962 toward the detection of glucose for patients with diabetes. Around the world, reliance on laboratory-based diagnostics for many diseases often presents a barrier to patients. In exchange for extreme precision and accuracy of measurements, such techniques tend to be expensive and housed in centralized facilities. Low-cost and location-agnostic alternatives continue to be explored for procedures such as biopsies, which are colloquially associated with cancer but can be employed for a variety of other health matters. A standard biopsy requires the extraction of a solid tissue sample, but biosensors have been strong candidates for *liquid* biopsies, the less invasive detection of physiological biomarkers in fluids like blood for diagnostic purposes. To this end, ongoing research is being conducted to evaluate biosensor operation in complex biological media. Whether for cancer, diabetes, cardiovascular disease, or a comprehensive health assessment, the biosensor is on track to become a versatile platform for the detection of biomarkers in liquids to manage a range of health conditions.

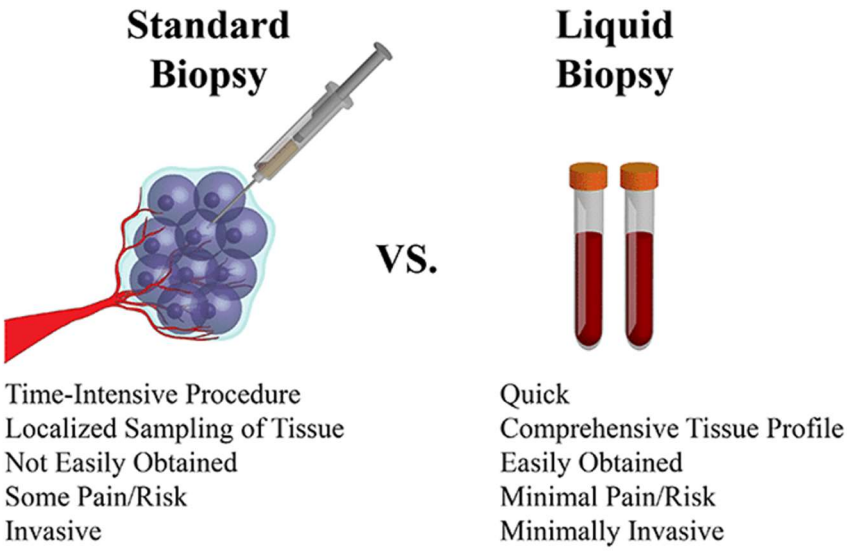

Figure 1. Standard biopsy vs. liquid biopsy. The comparative advantage of the liquid biopsy makes the technique an attractive option for diagnostic applications. From My Cancer Genome [1].

1.1 ALTERNATIVE DETECTION METHODS

Standard biopsies require a tissue sample collected at the site of the suspected cancer or affected organ using invasive procedures like endoscopic, needle, skin, and surgical biopsies [2]. Thin slices of the tissue sample are stained then placed under a microscope to determine the aggressiveness of the cancer or extent of any organ damage from disease or lifestyle behaviors [2]. The process can take several days to receive results, and there is no guarantee the sample was collected at the precise location of the damaged tissue [2]. However, tumors and stressed organ systems produce biomarkers that circulate in biological fluids throughout the body. The term "liquid biopsy" was coined in 2010 for analyzing circulating tumor cells in the blood of cancer patients [3]. Although venipuncture (blood draw) is also an invasive method, it is a safer, simpler, and more routine procedure which makes it less risky in comparison to tissue sample collection. Blood is not the only medium to collect a sample for a liquid biopsy, but it holds the most diagnostic potential and typically higher concentrations of biomarkers compared to other bodily fluids. Liquid biopsies were not initially intended as replacements for standard biopsies, but as complementary analyses for preventative screening, early diagnosis, patient treatment, and disease characterization such as understanding the heterogeneity of tumors [4]. The biopsy has its roots in cancer, but biosensors have always been studied for their potential to detect biomarkers for health conditions including Alzheimer's and cardiovascular disease. More recently and notoriously, the coronavirus pandemic that started in 2019 heavily relied on the power of biosensors to mitigate the spread of the virus. The ability to detect physiologically relevant biomarkers in biological fluids using alternative and novel methods is critical for the future of accessible diagnostics, disease characterization, and the more attentive management of health across populations.

1.2 OVERVIEW OF BIOSENSOR OPERATION

1.2.1 THE DEFINITION OF A BIOSENSOR

A biosensor is a device that measures biological or chemical phenomena by generating signals in proportion to the concentration of an analyte produced by a detectable event [5]. To accomplish this, a system is created consisting of a recognition element, transduction mechanism, and signal output. The recognition element captures the relevant parts from the sample (analyte) and triggers the signal transduction mechanism that creates a measurement to output. Upstream and downstream processing using electronics are often vital components of the overall system.

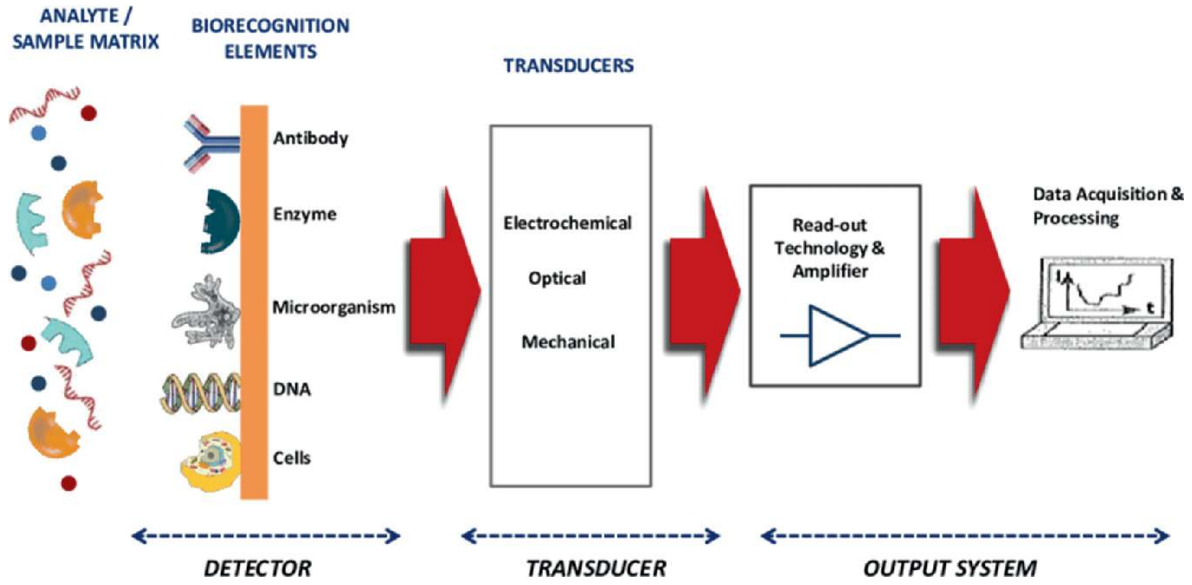

Figure 2. Components of a biosensor system. The recognition element is a critical aspect of biosensor design, as it initiates the signal and serves as the bridge between the analyte and transduction mechanism. From Bag *et al* 2022 *Next Generation Smart Nano-Bio-Devices*, reproduced with permission from Springer Nature [6].

There are many types of transduction mechanisms as well as recognition elements, but henceforth the focus will be on biosensors utilizing affinity-based detection, which is often contrasted with electrochemical detection.

ELECTROCHEMICAL BIOSENSORS – Electrochemical biosensors rely on electrochemical reactions to produce signals. A popular example is the glucose biosensor used in

diabetes management. The analyte (glucose) binds to the recognition element (glucose oxidase enzyme) functionalized on the surface of an electrode. This chemical reaction causes a transfer of electrons, and that resulting current is the mechanism of signal transduction used to quantify the binding phenomena. The magnitude of the electron transfer corresponds to a specific concentration of glucose in the sample, and that concentration is communicated as a measurement to the user via optical display. Electrochemical biosensors are the most prevalent systems studied across the literature and have widespread use in commercial applications.

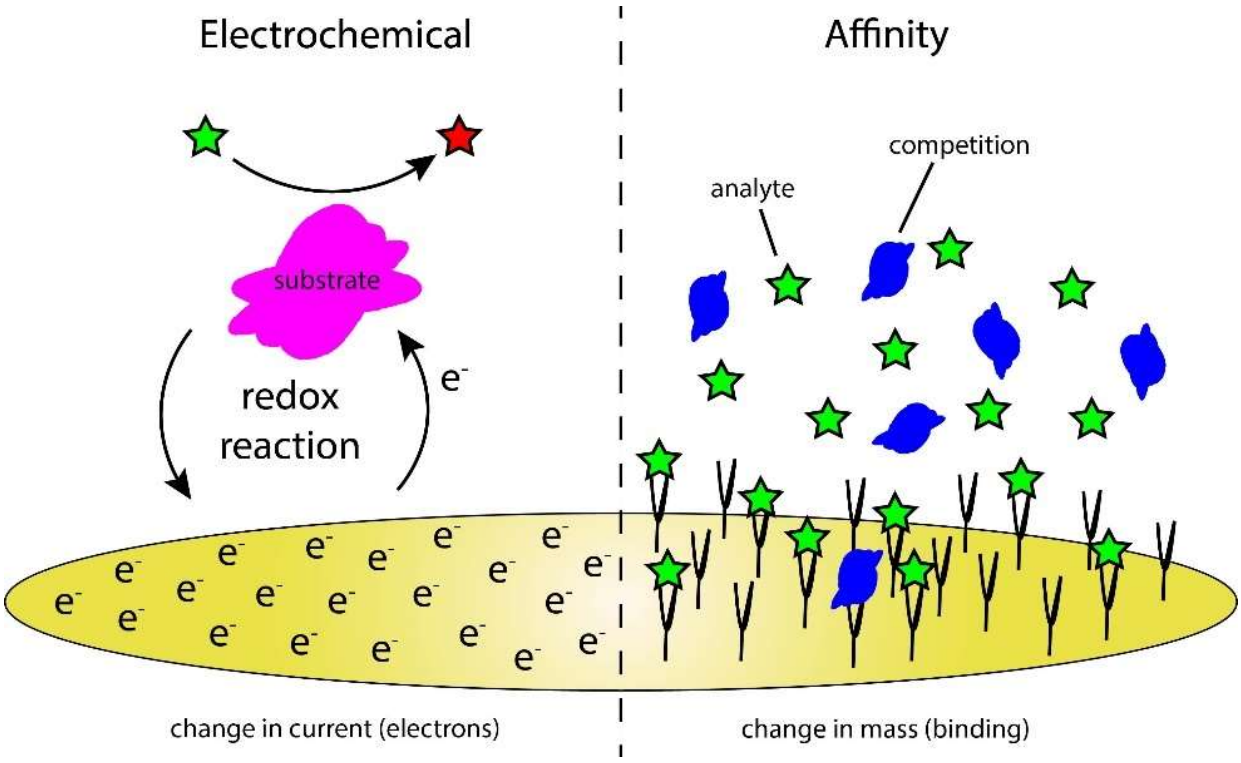

Figure 3. Electrochemical vs. affinity-based biosensors. Electrochemical and affinity biosensors utilize drastically different means of signal transduction to detect analytes.

AFFINITY BIOSENSORS – Affinity-based biosensors rely on the attractive forces between molecular species to produce signals. These species structurally complement each other and induce conformational changes as the binding complex forms between the analyte and recognition element. There are many examples, such as a biosensor developed to detect C-reactive

protein (CRP) in the body to assess inflammation, which is an analyte indicative of organ stress [7]. This biosensor may be functionalized with anti-CRP monoclonal antibodies as the recognition element on a surface, and CRP introduced to the biosensor within a sample would attach akin to puzzle pieces as the molecules bind to one another. The conformational changes on the biosensor due to the newly formed binding complex initiate a signal response that can be transduced in a variety of methods. If the CRP biosensor employed gravimetry as the transduction mechanism such as with microbeam resonators, the output measurement would convey an increase in mass due to the CRP analyte loaded on the surface [8]. Affinity biosensors are a popular choice for environmental monitoring, process analytical technology, and clinically as immunosensors for their diagnostic potential [9].

1.2.2 FUNDAMENTAL LIMITATIONS OF BIOSENSORS

The efficacy of a biosensor is only as optimized as its fundamental design. Therefore, careful consideration needs to be made when constructing the components of a biosensor system for detection. Many internal and external factors play key roles in determining signal integrity and performance expectations for a given biosensor system.

SAMPLE DETECTION – The concentration of analyte in the sample needs to be within the dynamic range of the biosensor. Problems with measurements arise when the quantity of analyte is outside the operational bounds, whether below the limit of detection, over the saturation limit, or in a nonlinear range of detection. Furthermore, the recognition element could be impacted by competitor species in the sample, reducing or confounding the true signal output due to lack of biosensor selectivity.

SAMPLE COLLECTION – The biosensor must work around any constraints for the production, capture, and analysis of commonly used fluids like urine, blood, sweat, saliva, and

tears. Laboratory-based diagnostics utilize substantial amounts of sample (e.g. urine in a cup for comprehensive urinalysis) since that is the required amount to make an accurate measurement. A poorly designed biosensor system using complex biological media could require more volume than is practical to make an effective measurement.

SYSTEM DEGRADATION – The fouling of biosensor components over time drastically impacts the quality of measurements and influences the need for maintenance and replacement. Complex biological media contains a lot of "junk" that can attach itself to the biosensor surface including proteins, cells, and other biological materials [10]. Even though the recognition element is inherently consumed as a result of normal biosensor operation, excess materials on the surface hinder the detection of the analyte and overall system performance. Thus, the operational life of a biosensor is often determined by the surrounding environment or any harsh conditions the system is subjected to. Calibration data typically captures the biosensor fouling behavior which can be deduced by the linearity of the response over time or over multiple cycles of use.

OPERATIONAL LIFETIME – The biosensor system can only be effective for a specified utility or length of time by design. Biosensors may be characterized by their intent to be single-use, multiple-use, or continually used, in which measurements are taken over a certain span of time. Modern glucose biosensors operate for up to two weeks, and this extended runtime has been pivotal for diabetes management. Optimal management of health requires longitudinal monitoring, so it is important for a biosensor system to operate as reproducibly and as long as possible to be practical for consumer applications. Biosensor design also calls for power, size, and comfort considerations, but the recognition element should always be constructed to operate over a relevant timespan and predetermined total quantity of analyte.

1.2.3 CHARACTERIZATION METHODS OF BIOSENSORS

Various approaches are used to characterize biosensor systems for efficacy and performance. It is important to note that not all researchers characterize biosensors in the same manner, and there have been calls for standardization across the literature. Regardless, characterization data is necessary to compare and replicate results for a more accurate understanding of the capabilities of a biosensor system design.

FUNCTIONALIZATION – Functionalization refers to the chemical preparation procedure that enables a biosensor to make experimental measurements. The structure and functionality of the recognition element on the biosensor surface needs to be verified, as well as a reasonable approximation of the density or number of sites available for detection. Without this knowledge there is less certainty in the signal output. Common surface analysis techniques include fluorescence, goniometry, ellipsometry, atomic force microscopy, scanning electrode microscopy, mass spectrometry, and gravimetry. The biosensor surface would be characterized starting with the blank surface as a control, after each additive step throughout functionalization, and during an experiment to analyze the unperturbed surface pre-sample and then post-sample with the analyte bound to the recognition element. Every step should demonstrate distinct and perceivable differences regarding the surface characteristics, and multiple techniques are often used in conjunction to add robustness to conclusions. The information provided by such techniques is also utilized to determine structural stability and biosensor shelf life.

SENSITIVITY – The sensitivity of a biosensor signal response and its dynamic range of operation are defining measurement properties. The minimum amount of analyte that can be detected by a biosensor is known as the limit of detection, which was introduced as a potential limitation of biosensors [5]. The limit of detection is often the first indication that a biosensor is

performing because the measurement will start to differentiate in its signal output at this point. On the opposite end of the spectrum, the saturation limit is the point at which the signal stagnates in its response due to being at capacity. Between these two points is the dynamic range of the biosensor, which is further characterized by the signal resolution and signal-to-noise ratio (SNR). The resolution of a biosensor is depicted by its linearity, a measure of the relationship between increasing concentrations of analyte and the impact on signal output. A biosensor with high resolution and linearity will demonstrate greater changes in signal produced by smaller quantities of analyte (steeper slope) as it is more sensitive. SNR is the measure of the amplitude of the desired signal to the level of background noise [11]. This ratio contributes to the evaluation of biosensor performance, as changes in signal amplitude often correspond to changes in noise that could impact the biosensor system measurements [12]. Biosensors that can operate both in air and liquids have this problem, showing a significant decrease in SNR due to liquid damping, thus reducing the sensitivity of the biosensor system.

SELECTIVITY – Selectivity is the ability of the recognition element to bind and select for a particular analyte in a sample that contains competitor species and other contaminants. Thus, the choice of the recognition element has the most direct impact on the selectivity of the biosensor. For affinity biosensors, aptamers and antibodies are commonly used recognition elements. Aptamers are highly selective, more stable, have a longer shelf life, and result in the strongest attractive binding forces although antibodies have been and still are the traditional choice in research studies [13, 14]. Selectivity is often confused with specificity, which is the ability of the recognition element to only be able to bind with a particular analyte.

REPRODUCIBILITY – A biosensor system utilizing the same setup and conditions needs to produce predictable responses over multiple cycles or lengths of time. Identical results

should be produced by two completely different biosensors manufactured using the same methods. Reproducibility is often influenced by the stability of the biosensor components and is typically a testament to the selection of a reliable recognition element and the robustness of the overall biosensor system design.

1.2.4 NEXT-GENERATION BIOSENSOR APPLICATIONS

Advancements in biosensor technology are the result of overcoming previous limitations and opening the door for new paradigms in biosensing techniques and applications. "Next-generation" is often used as a buzzword to describe significant progress – miniaturization, enhanced sensitivity, faster responses, and higher throughput are just a few of the many improvements that fall under this category [15]. For example, miniaturization ushered in microfluidics and the age of lab-on-a-chip. Miniaturization has also enabled biosensors to become more portable, leading to the field of wearable devices. Enhanced sensitivity is key for clinical applications, and the development of aptamers has challenged the widespread reliance on antibodies as recognition elements. Faster responses allow mitigation strategies to be implemented before circumstances worsen, whether for contamination in therapeutic drug production lines or preventing the spread of diseases like coronavirus and sexually transmitted infections. Higher throughput and simultaneous measurements are critical for biosensor robustness and facilitating much more comprehensive analyses and diagnostic utility. Hereafter, the discussion of next-generation biosensor applications will center on biosensor regeneration and arrayed detection.

BIOSENSOR REGENERATION – As mentioned in an earlier section, the recognition element is consumed over the course of normal biosensor operation as the analyte binds to the surface and initiates a signal. Biosensor regeneration involves detaching the analyte from the recognition element so that the detection site and overall biosensor can be used once again. This

is beneficial for numerous reasons such as tunable detection, reduction of sensor-to-sensor variability, and extending the operational lifetime of biosensors by supporting multiple cycles of measurements. Biosensor regeneration is possible because the affinity-based interactions between the analyte and recognition element are the sum of spontaneously favorable forces. Although aptamers are heralded for their selectivity and specificity, the extremely attractive binding forces between aptamer pairs prevent them from being practical choices as recognition elements to enable biosensor regeneration. Recognition elements such as peptides and antibodies have comparatively less attractive binding forces and are thus prime for exploring methods of dissociating analytes from biosensor surfaces.

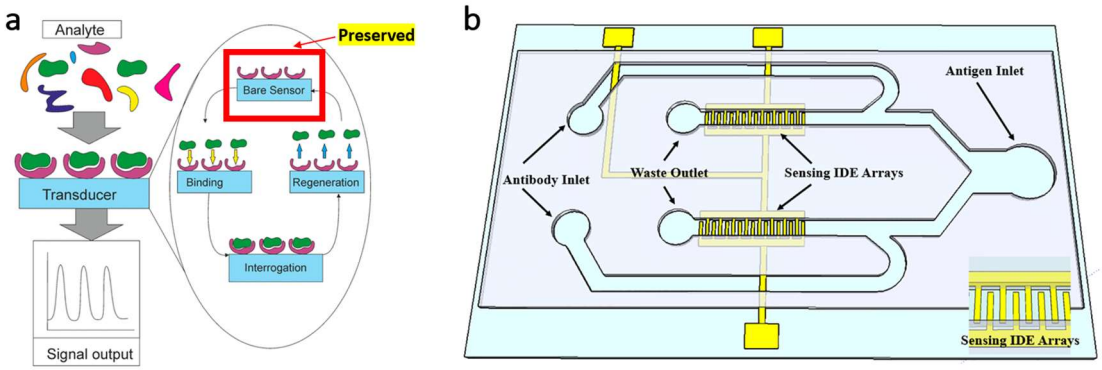

Figure 4. Next-generation biosensor applications. (a) Biosensor regeneration preserves the original recognition element (boxed in red on the bare sensor) throughout multiple cycles of detection. Adapted from Goode *et al* 2015 *Langmuir*, with permission from the American Chemical Society [16]. (b) Arrayed biosensors increase the throughput of measurements via multiple detection regions. From Liu 2019 [17].

Favorable dissociation conditions that reverse the spontaneity of affinity-based binding can be attributed to enthalpic, entropic, chemical, thermal, and electrochemical factors as overviewed by Goode et al. [16]. Enthalpic interactions depend on the thermodynamic stability of the system which can be changed by manipulating ionic strength, pH, or competitor species in the solvent environment. Entropic interactions rely on the tendency toward disorder, such as using a detergent to disrupt a hydrophobic amino acid recognition element. Chemical interactions for biosensor

regeneration induce harsh conditions like high or low pHs to disturb the binding complex, but such conditions can be particularly damaging to biosensor components. Thermal regeneration techniques elevate temperature to allow kinetic energy to overcome the binding forces on the biosensor. Lastly, electrochemical regeneration applies negative potentials across the biosensor surface plane to create highly localized environments and control analyte desorption.

ARRAYED DETECTION – The analytical capabilities and throughput of a biosensor system increase with additional regions for detection. Most biosensors only measure for one particular analyte, whereas arrayed setups enable replicate measurements of a variety of analytes at the same time [18]. Furthermore, more information is captured in less time and only a single sample is needed, which mitigates some limitations of biosensors. Each detection region has its own set recognition element, and the signal is transduced through the same biosensor system. Arrayed biosensing can potentially add complexity to systems due to signal interference and crosstalk, requiring more in-depth electronics and signal processing for the biosensor. However, arrayed biosensing techniques and applications hold a lot of promise as the cost-effectiveness and utility of the method are indisputable.

Next-generation biosensors will be necessary to overcome the limitations of operation and enhance the characterization of analytes in complex biological media, as well as for demonstrating the practicality of biosensor technology for various applications. In this body of work, a resonance-based biosensor was developed, inspired by the prospect of biosensor regeneration and arrayed detection toward changing the landscape of monitoring personal health and disease management.

1.3 RESONANCE-BASED BIOSENSORS

Resonance-based biosensors use frequency as a mechanism of signal transduction. All materials naturally oscillate at their resonant frequency, which is a property intrinsic to the

chemical and structural makeup of a material. When the conditions of said material are manipulated, the resonant frequency of the material also changes, which is the basis of how resonance is used to transduce signals as a biosensing technique. Many resonance-based biosensors rely on surface chemistry and the properties of thin films, requiring a material or methodology with a resonant frequency range sensitive enough to detect phenomena invisible to the naked eye. Quartz is a popular example in biomedical applications, with the quartz crystal microbalance (QCM) biosensor able to detect mere nanograms of analyte on its surface depending on the cut and thickness of the crystal. The QCM was selected as the biosensor of choice in this body of work for reasons explained later in this section, however, there are a handful of other biosensors that exploit similar principles of resonance through slightly different means of transduction.

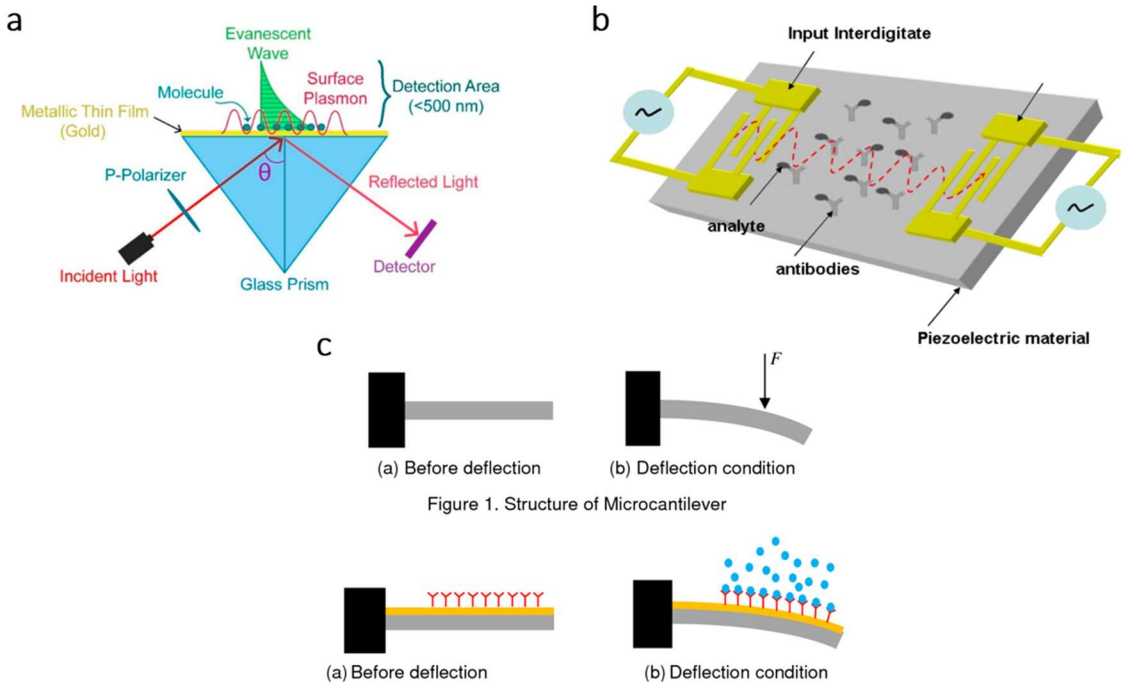

Figure 5. Examples of resonance-based biosensors. (a) Surface plasmon resonance (SPR) biosensors rely on the frequency of plasmons coupled to a functionalized surface. From Eddin 2020 [19]. (b) Surface acoustic wave (SAW) biosensors are based on the frequency of waves that propagate between two electrodes across a functionalized surface. From Zhou 2012 [20]. (c) An example of micro-electromechanical systems (MEMS) biosensors is the micro-cantilever beam, which uses the frequency of deflection to determine the mass loaded on a functionalized surface. From Febriansyah 2012 [21].

SURFACE PLASMON RESONANCE – the transduction mechanism for surface plasmon resonance (SPR) biosensors utilizes the fundamentals of refraction and interactions of light. An optical light source is directed into a prism on top of a metal surface functionalized with recognition elements. After flowing the sample through the biosensor system causing analytes to bind to the surface, the refractive properties of the surface change. This has an impact on the penetration of the light source and induces shifts in the angle and intensity of the light as it reflects toward the detector on the opposite side [22]. The output is unitized at 0.0001 degrees of an angle, and the inherent resonance of SPR arises from the quantity of light that couples and propagates through the metal surface at a certain angle of incidence. These "plasmons" oscillate at defined angles and wavelengths (frequencies) depending on the material near the surface (i.e., analyte) [23]. Since the binding of analytes can cease the oscillation of the system, the physical interactions and amount of reflected light are instead used for signal quantification [23].

SURFACE ACOUSTIC WAVE – the transduction mechanism for surface acoustic wave (SAW) biosensors utilizes the piezoelectric effect of materials like quartz, where electrical stimulation causes oscillatory mechanical stress (vibrations) at the resonant frequency. These oscillations create thin film waves across a surface between electrodes at specific modes of acoustics (Rayleigh, shear horizontal, Love, and Lamb waves) [24]. The selection of an acoustic mode is based on the thickness of the piezoelectric material or determined by biosensor design requirements such as the need for liquid propagation [25]. SAW biosensors typically employ interdigitated electrodes and additional chemicals as wave-guiding layers, which add to their complexity [26]. The surface between the electrodes is functionalized with recognition elements, and as the sample is introduced to the biosensor which causes analytes to bind to the surface, the

frequency of the wave propagating between the electrodes is impacted. The ensuing shift in the resonant frequency of the system is the means of signal quantification.

MICRO-ELECTROMECHANICAL SYSTEMS – the transduction mechanism for micro-electromechanical systems (MEMS) biosensors vary widely, but this classification of biosensors relies on microscopic mechanical structures embedded with electronics, and recognition elements functionalized on said structures [27]. The most widespread example is the cantilever, a suspended micro-scale beam balance structure which can freely deflect on one end, typically fabricated through photolithography. The vibration of the beam is the natural resonance of the structure and can be induced through electrical, thermal, or acoustic actuation [28]. When analytes bind to the surface of the functionalized mechanical structure, the shift in resonance is transduced via the changes in the mechanical properties of the system (e.g., the beam deflects at a slower frequency) which is how the signal is quantified.

Another example of a MEMS biosensor is the microneedle for transdermal biomarker detection. These biosensor devices are designed with absorptive sample collection capabilities in addition to traditional sample analysis. Microneedle patch structures painlessly puncture the skin and uptake interstitial fluid toward the sampling region of the biosensor [29]. The analytes then bind to the recognition element and the signal is transduced, processed, and output through embedded electronics. Microneedle biosensors face challenges due to difficulties surrounding micromachining techniques and reproducibility, however, these MEMS continue to be studied owing to their potential to mitigate the invasiveness of the blood draw especially for applications in continuous glucose monitoring [29]. Microneedles are more of a MEMS structure than a resonance-based technique, but researchers have demonstrated integrations with plasmonic nanocomposite transducers for on-patch optical analysis similar to the principles behind SPR [30].

1.3.1 THE QUARTZ CRYSTAL MICROBALANCE

Only a few resonance-based biosensors have been studied as extensively as the QCM for biosensing applications in gases and liquids. The QCM is comprised of a circular or rectangular flat quartz crystal with electrodes on both sides. As quartz is a piezoelectric material, electrical excitation across the electrodes causes the crystal to vibrate, and the frequency at which the most signal passes through (highest SNR) is the resonant frequency. This frequency is characterized by the Q factor, a measure of the bandwidth and amplitude of the resonant peak. The resonant frequency of the quartz is largely defined by the thickness of the crystal and can be cut along certain axes to impact sensitivity and temperature stability. For reasons of practicality, QCM crystals in biomedical applications tend to fall on the lower end of the 1-100 MHz range since the high frequency, more sensitive, and thinner crystals are relatively fragile to handle. Furthermore, thin crystals have weaker penetration depths in liquids, meaning the oscillations would not be powerful enough to overcome the viscous forces in the surrounding fluid to resolve a clear signal.

In its use as a biosensor, one of the QCM electrode surfaces is functionalized with the recognition element to contact the sample, whereas the electrode on the other side normally remains as is. The microbalance nature of the biosensor is due to gravimetry as the transduction mechanism – the analytes binding to the recognition element add mass to the electrode surface which increases the weight of the QCM, slowing the oscillations and decreasing the frequency of the crystal vibrations. In liquids, the addition of mass is represented by an increase in the viscosity of the thin film layer above the surface. The resultant shift in resonant frequency is used to quantify the mass on the biosensor surface due to the binding phenomena and mass loading of the analyte.

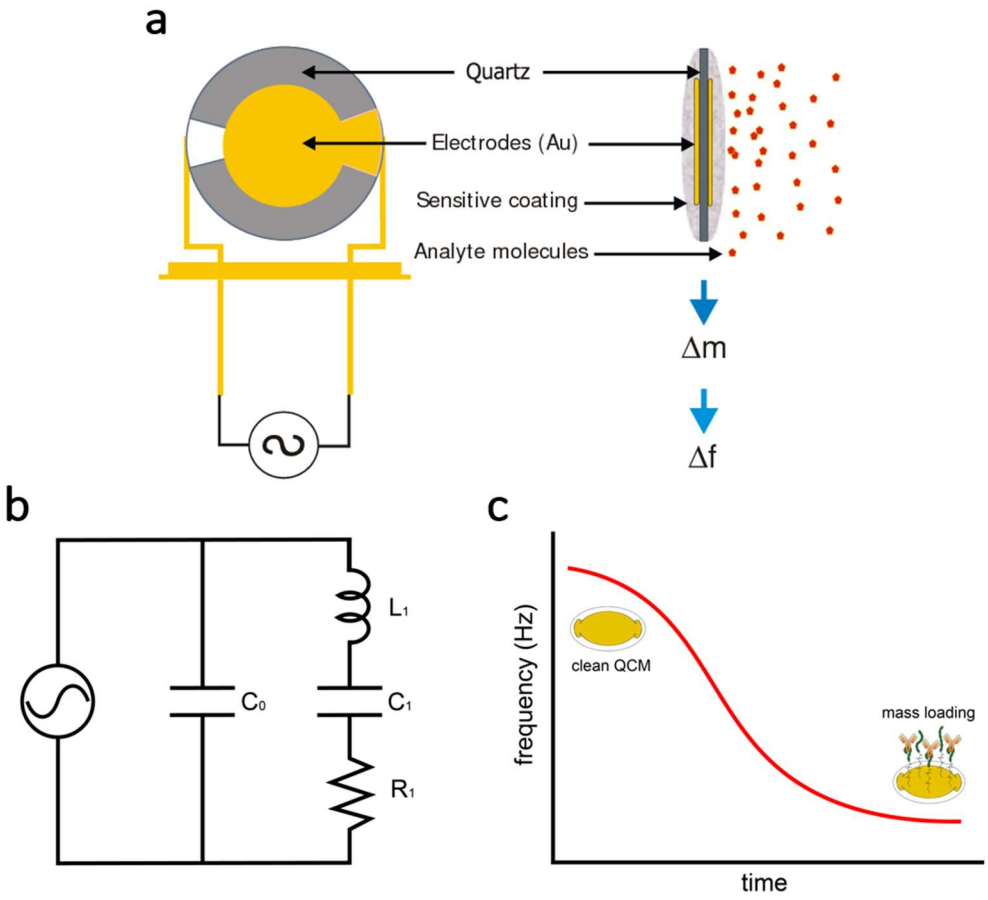

Figure 6. Principles of the quartz crystal microbalance (QCM) biosensor. (a) A quartz crystal with a functionalized electrode makes use of piezoelectricity and gravimetry to transduce loaded mass into a shift in frequency. From Yuwono 2004 [31]. (b) The Butterworth-Van Dyke (BVD) equivalent circuit is often used to model the QCM. (c) The final representation of the QCM signal is usually depicted by a decrease in frequency as mass loads to the surface over time.

Günter Sauerbrey first demonstrated the use of a quartz oscillator as a mass sensor for his doctoral thesis in the 1950s, formulating the Sauerbrey equation (Equation 1) as a depiction of the relationship between the resonant frequency of quartz and a mass loading on the surface [32].

$$\Delta f = -\frac{2{f_0}^2}{A\sqrt{\rho_q \mu_q}}\Delta m$$

Equation 1. Sauerbrey equation. In this equation, f is the normalized frequency (Hz), f_0 is the resonant frequency (Hz), A is the area of the electrode (cm^2), ρ_q is the density of quartz (g/cm^3), μ_q is the shear modulus of quartz ($g \cdot cm^{-1} \cdot s^{-2}$), and m is the mass (g) [32].

Considering f_0, A, ρ_q, and μ_q remain constant, the change in mass (Δm) is directly proportional to the change in the frequency (Δf) of the system. It is important to note that the Sauerbrey equation was intended for QCM operation in air, and the sensitivity and resolution of this relationship is highly dependent on the thickness and cut of the crystal as well as the medium surrounding the QCM. A 5 MHz AT-cut quartz crystal has a theoretical mass sensitivity of 17.7 ng/cm^2 per 1 Hz change in frequency, but some applications in the literature with unique biosensor designs have shown the QCM to exhibit enhanced sensitivities by measuring picograms of analyte [33, 34]. However, the same cannot be said for many liquid applications, as QCM biosensors used in liquid media have been shown to amplify some of the limitations regarding biosensor operation, and new models needed to be formulated to accurately describe the frequency relationship [35].

$$\Delta f = -{f_0}^{3/2}\left(\eta_l \rho_l / \pi \rho_q \mu_q n\right)^{1/2}$$

Equation 2. Kanazawa and Gordon equation. In this equation, f is the normalized frequency (Hz), f_0 is the resonant frequency (Hz), η_l is the absolute viscosity of the liquid (cP), ρ_l is the density of the liquid (g/cm^3), ρ_q is the density of quartz (g/cm^3), μ_q is the shear modulus of quartz (g·cm^{-1}·s^{-2}), and n is the mode number of oscillation [36].

The Kanazawa and Gordon equation (Equation 2) was named after the two scientists who first studied QCM operation in contact with liquids [36]. In these conditions, a change in mass correlates with changes in the viscosity (η_l) and density (ρ_l) of the liquid in contact with the functionalized electrode surface. The assumptions for the validity of this equation are the following: the piezoelectric crystal is a perfectly elastic solid, the contact liquid is Newtonian, and the liquid can be approximated to a semi-infinite layer [37]. It is also a requirement that either one or both electrodes on opposite sides of the crystal are completely immersed in the liquid (most applications only submerge one side). The Kanazawa and Gordon equation is not the only means used to characterize the QCM in liquid media, given that the Butterworth-Van Dyke (BVD)

equivalent circuit is used as a starting point for many other viscoelastic models. Biosensor operation in liquid media reduces the SNR compared to dry operation in vacuum or air, and this is especially true in the case of the QCM as seen by a significant reduction in Q factor. Biosensor operation in liquids is still not fully understood for the QCM, as many have observed positive frequency shifts after the coupling of analytes to the surface, and the need for "warm-up" periods to stabilize the QCM prior to taking measurements [38-40].

RECENT ADVANCES WITH QCM BIOSENSORS – The QCM has been studied by many across the literature as a platform for exploring and expanding biosensor capabilities due to its relative ease of construction and versatile design – the only requirements being a flat piece of quartz and electrodes on both sides which can be patterned a multitude of ways. One study highlighted concentric ring electrodes being able to increase sensitivity and performance while reducing overall size and minimizing interference between electrodes [41]. Another study showed a monolithic QCM for simultaneous detection of a virus with as many detection regions as space allowed [42]. Arrayed QCM fabrication is a popular approach for demonstrating the creativity and potential of the QCM for multiplexed biosensor applications.

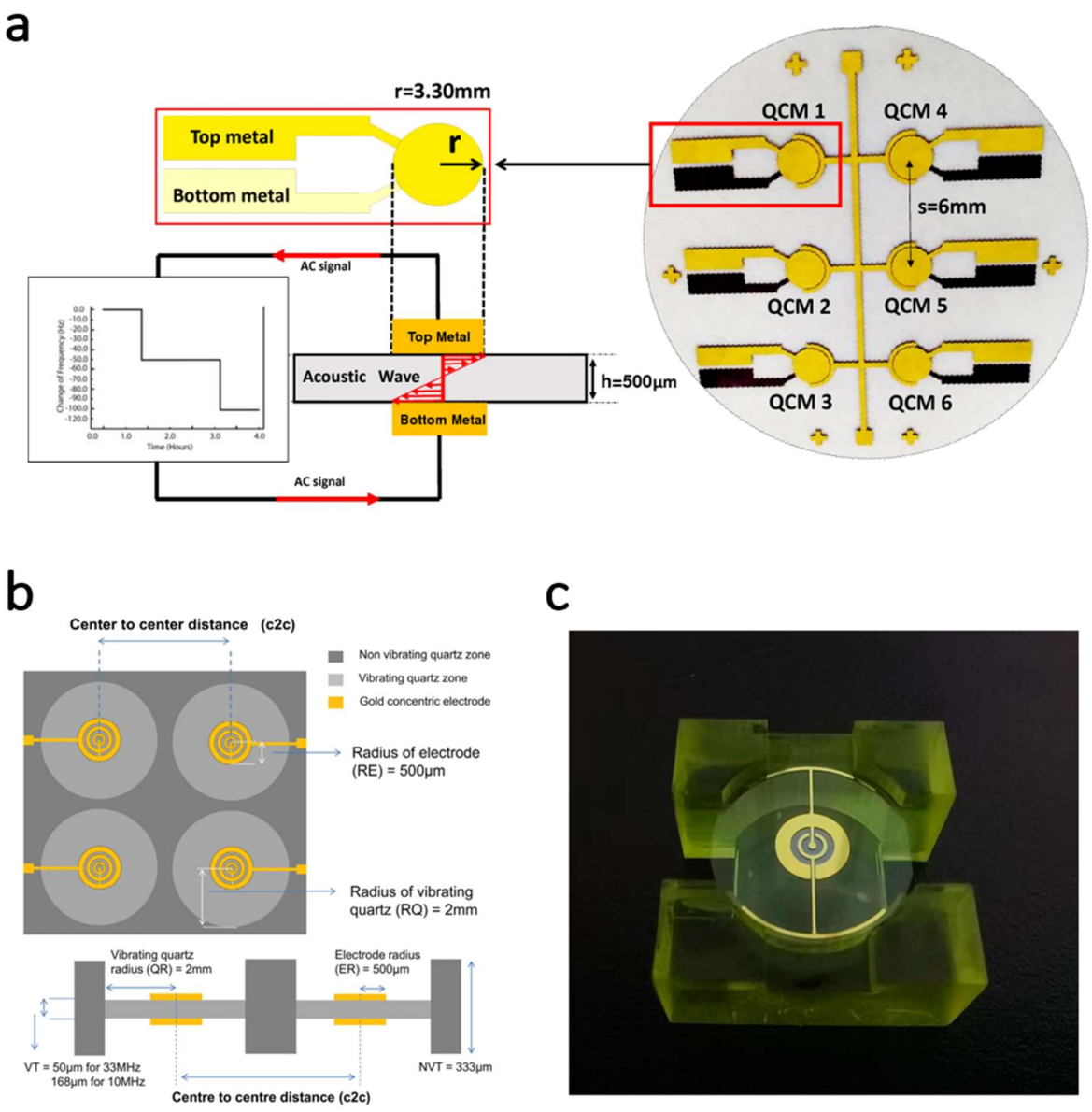

Figure 7. Examples of enhanced QCM biosensors. (a) Monolithic arrayed QCM biosensor design with six regions for detection. From Zainuddin 2018 [43]. (b) Theoretical concentric ring electrode QCM biosensor design to overcome the disadvantages of non-uniform mass sensitivity. From Joseph 2020 [44]. (c) Fabricated ring-shaped interdigitated electrode QCM biosensor design to maintain uniform mass sensitivity. From Wang 2022 [41].

The QCM has also received a lot of attention in biosensor regeneration studies. Goode et al. suggested six criteria for successful biosensor regeneration: baseline restoration, signal loss between cycles, integrity of the recognition element, at least 10 cycles of continual measurements, explicitly stated regeneration conditions, and a signal loss profile for calibration throughout the

lifetime of the biosensor [16]. Most examples across the literature utilize chemical regeneration schemes to dissociate the analyte from the recognition element and regenerate the biosensor. Nonetheless, the property of quartz being a piezoelectric material has the potential to be exploited. It is well understood that analytes binding on the functionalized electrode surface shift the resonant frequency of the QCM biosensor due to changes in the system. The nuanced reversal of that process is to manipulate the frequency of the system to induce changes on the electrode surface, disrupting the analyte binding complex interactions with the intention of regenerating the recognition element. Furthermore, for tunable detection if certain biological materials or conformations respond to specific frequencies, then biosensor selectivity can be controlled, reducing the impact of competitor species and contaminants on limiting biosensor performance. The work in this thesis constitutes the fundamental initial steps toward the bigger picture concepts of regeneration through resonance as well as enhanced biosensing through arrayed detection. These concepts served as the inspiration for why the QCM was chosen in this body of work – manipulating the amplitude and frequency of the quartz has an unknown and unstudied impact on surface chemistry and molecular interactions. A next-generation biosensor with such features will be critical for analyte detection in complex biological media, as it requires a much deeper understanding of the phenomena driving these systems to enable their mastery and control.

2. SYSTEM DESIGN

Toward the development of a QCM biosensor for next-generation detection of analytes in complex biological media, AT-cut quartz crystals were purchased from openQCM (Pompei, IT) in 5 MHz and 10 MHz configurations, with theoretical mass sensitivities of 17.67 $ng \cdot Hz^{-1} \cdot cm^{-2}$ and 4.42 $ng \cdot Hz^{-1} \cdot cm^{-2}$, respectively [45, 46]. The AT cut of quartz has acceptable signal stability (1-3 Hz/°C) at room temperature, so it is a popular choice across the literature [33]. Although the 5 MHz crystal is the least sensitive of the two configurations, it was the main choice due to suggestions that these crystals are better suited for liquid applications considering their comparative resiliency against viscoelastic losses [47]. The 5 MHz QCM had a thickness of approximately 270 μm, a diameter of 13.95 mm, and 200 nm thick gold electrodes on each side. The bottom electrode diameter was 5.6 mm, and the larger top electrode meant for the liquid interface had a diameter of 11.2 mm, each with an additional 10 nm of titanium substrate for electrode adhesion. Both electrodes wrapped around the edges of the crystal to allow for single-sided contact with spring-loaded (pogo) pins. Herein, the development of this QCM into a biosensor system will be discussed by overviewing the selection and functionalization of the recognition element, the integration of electronics and microfluidics, and the experimental instrumentation powering the overall system.

Figure 8. AT-cut QCM purchased from openQCM. Top and bottom of the crystal used for QCM binding experiments [45, 46]. The larger top electrode contacts the liquid sample, and the electrodes overlap in the middle which creates a sensitive region.

2.1 SURFACE FUNCTIONALIZATION

ANALYTE: IMMUNOGLOBULIN G – Immunoglobulin G (IgG) is the most common antibody found in the body, and serves to protect against pathogens by identifying previously exposed infectious agents and initiating new immune responses [48]. Thus, increased levels of IgG are normally indicative of allergies or infections, but have also been seen with cancer, autoimmune disorders, and other diseases [48]. Low levels of IgG can indicate a weakened immune system and increase the susceptibility of a person getting sick [48, 49]. The structure of the IgG molecule (Figure 9) consists of multiple polypeptide chains and is depicted as a flexible Y-shaped structure [50]. Since IgG molecules are important for immunogenicity (the ability of the body to prompt an immune response), they are often used for the development of therapeutics [51]. Such applications were first implemented in the 1980s when mouse antibodies were extracted and used as immunosuppressive agents during organ transplantations [52].

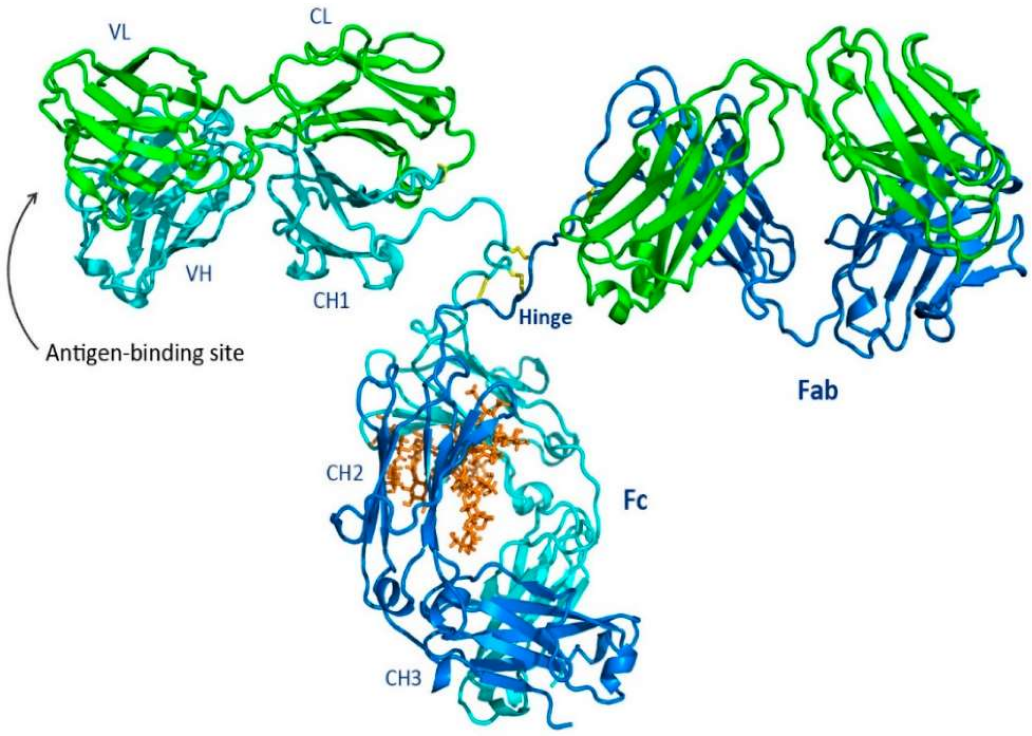

Figure 9. Molecular structure of the immunoglobulin G (IgG) antibody. The Y-shaped structure of IgG is a common depiction of the molecule. From Chiu 2019 [53].

The genetic modification of IgG molecules for specific targets has the potential to treat a range of diseases and health conditions. This has been accelerated through industrialization processes and the development of recombinant manufacturing technology. IgG is classified as a monoclonal antibody (mAb), meaning that large quantities of identical molecules can be synthesized with a pre-selected specificity via recombinant DNA methodology [54]. The relevant genes from the antibody's Y-shaped structure are extracted, then viruses are used to transfect host cells for expression and rapid production providing an unlimited supply of mAb molecules [55, 56]. However, this process is not perfect as contaminants can reduce the ultimate purity of the product and resulting efficacy of the therapeutic drug, especially at the industrial scale. Biosensors for IgG detection have been explored in this capacity to measure both contaminants and concentrations of product during the therapeutic drug development process, using inline measurements to mitigate impacts on the inherent costs and quality of operations. Thus, the enhanced capabilities of biosensor regeneration and arrayed detection are prime for applications such as the characterization of product attributes in a non-invasive manner, which was another thrust of the research in this body of work. IgG was selected as the model analyte for the QCM biosensor, with the intention to explore other analytes and biomedical applications in the future.

BIOSENSOR CLEANING & FUNCTIONALIZATION – manufacturers and distributors often place the QCM crystals in individually wrapped sleeves during the shipping process, which was an impediment to ensuring the cleanliness of the gold electrode surfaces. Thus, vendors of QCM recommend a thorough cleaning process prior to biosensor functionalization and experimentation. The conventional method uses a harsh piranha solution (3:1 sulfuric acid to hydrogen peroxide), but this had the potential to damage the electrode and the underlying substrate adhesive layer [57]. Other methods follow strategies similar to the one described in the next

paragraph which was used in this body of work [58]. To preserve manufacturer conditions, the crystals were stored in their original packaging until they were needed for an experiment. The transfer of the QCM crystals across all steps was handled manually using metal tweezers along the quartz crystal edge.

The first step in cleaning the QCM was to wash the electrode surface by briefly squeezing different solutions using a wash bottle. First, acetone was washed over the QCM to remove dirt and impurities from the surface. Then, ethanol was washed over the surface followed by rinsing in ultrapure Milli-Q water. Some researchers sonicate the crystals or utilize UV/ozone treatment as an added measure. The QCM was then dried with nitrogen gas and placed in a glass vial for holding unless the surface was immediately ready to be functionalized. Otherwise, when the time came, the crystal was again washed with ethanol and Milli-Q water then dried with nitrogen gas prior to the first incubation step of the functionalization procedure.

To functionalize the gold electrode surface of the QCM, the principles behind self-assembled monolayers (SAM) were applied, which are well-ordered organic surfaces with controlled properties at the molecular interface [59]. The SAM was critical for the stability and availability of the recognition element and its utility as a surface-blocking agent, preventing the non-specific binding of competitor species to the gold electrode [60]. This process began by making a concentration (1 mg/mL) of thiolated poly(ethylene glycol) (HS-PEG 1000-NH2) (Figure 10) in ethanol solution. Once the thiol-PEG powder was dissolved, the solution was transferred to the glass vial containing the QCM. The solution was pipetted directly onto the gold surface, with enough volume to completely submerge the crystal on both sides. The QCM was left to incubate overnight in dark conditions at room temperature.

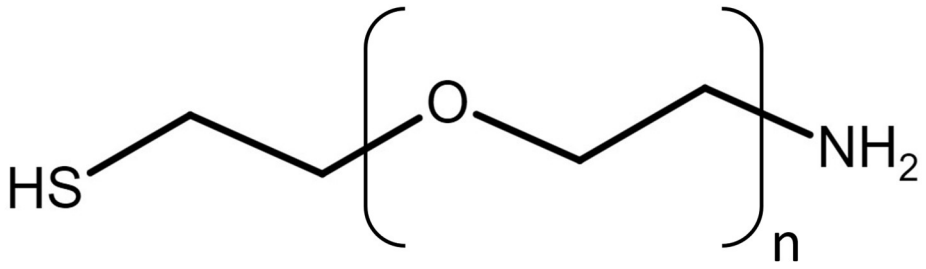

Figure 10. Molecular structure of thiolated poly(ethylene glycol). Produced using Chemical Sketch Tool [61].

The next layer of the SAM was the addition of the peptide (HWRGWV) that captures IgG, and this was accomplished through an EDC/NHS coupling reaction. A concentration (38.2 mg/mL) of EDC was made in MES buffer for one solution, and 1 mg of peptide was added to 1980 µL of MES for another solution. The EDC solution was vortexed to dissolve the powder, and the peptide solution was dissolved via pipette. 20 µL of the EDC solution was combined with 1980 µL of the peptide solution for a total volume of 2 mL, which was left to react for 10 minutes in dark conditions at room temperature. The QCM was washed with ethanol and Milli-Q water before being immersed in the final combined 2 mL peptide solution, then incubated for 1 hour in dark conditions at room temperature. Following the immobilization of the peptide, the QCM biosensor was considered functionalized and ready for experiments. As the final step if the QCM was not immediately used for an experiment, the QCM surface was washed with PBS and Milli-Q water, then immersed in PBS solution within a glass vial and placed in a fridge for holding.

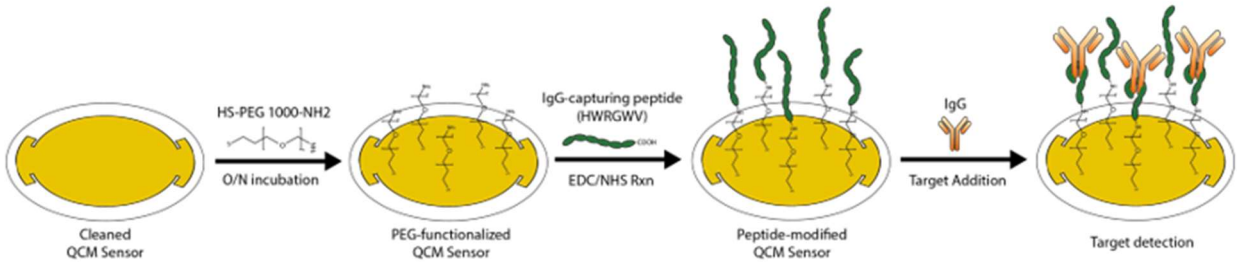

Figure 11. QCM biosensor functionalization procedure. Steps for orienting the peptide recognition element on the electrode surface. Courtesy of Dr. BangHyun Lee, BioInterface Lab.

PEPTIDE: HWRGWV – The hexamer peptide containing the amino acid sequence HWRGWV was used as the recognition element to capture IgG analyte in sample (Figure 12). As mentioned earlier in this section, IgG is an important molecule in the pharmaceutical industry for therapeutic drug development purposes, with large proteins such as Protein A and Protein G being used for downstream capture of IgG in production lines [62]. These large proteins have proven problematic since their three-dimensional structure may denature over repeated cycles of product capture and elution [62]. Proteins used in drug development processes are also expensive and can potentially increase the immunogenicity of the product [62, 63]. The desire for alternative methods or molecules that mimic the binding of IgG similar to large proteins has contributed to the exploration of peptides as an option for downstream affinity capture and detection [63, 64].

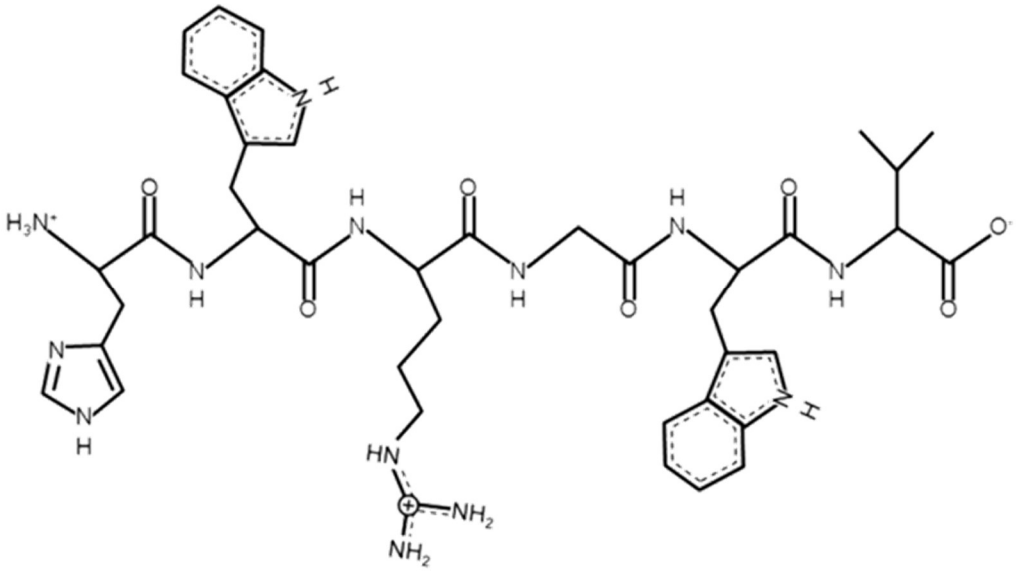

Figure 12. Molecular structure of the HWRGWV peptide. Produced using PepDraw [65].

In comparison to larger proteins, peptides such as HWRGWV are less immunogenic as synthetic molecules, more cost-effective, and more stable due to their structural linearity and lack of three-dimensionality [62, 63]. The mechanism of interaction between these smaller peptides and IgG remain largely unknown, but the data supports and shows the ability to efficiently capture

and isolate IgG from complex media and selectivity against other proteins [64, 66]. The HWRGWV peptide molecule attaches to the Fc fragment of IgG (Figure 9) in a manner similar to Protein A [62, 63]. The peptide was identified as a candidate through a one-bead-one-peptide combinatorial library screening technique using chromatography resins [66, 67].

One study used a set of three linear Fc-binding hexamer peptides (HWRGWV, HYFKDF, and HFRRHL) which share a common histology (histidine + aromatic patch + positively charged patch) to examine their selective absorption and isolation of human IgG via affinity chromatography [63]. Spiked samples (0.05 mg/mL – 10 mg/mL) of IgG in complete mammalian cell culture were used, and this complex medium comprised of Eagle's minimum essential medium with 10% fetal calf serum and 5% tryptose phosphate broth, resulting in a solution rich with amino acids, salts, and contaminants [63]. With regard to purity of product, HWRGWV had the highest at 90.9% compared to 86.7% and 88.6% for HYFKFD and HFRRHL, respectively [63]. When NaCl was added to the PBS buffer to remove non-specifically bound proteins, the purity for HWRGWV rose to 97.7% with a yield of 94.8%, with HYFKFD having 92% purity and 65.8% yield, and HFRRHL having 90.6% purity and 62% yield [63]. The HWRGWV peptide was comparable to Protein A in its considerable purity, yield, and recovery, and performed the best overall among the other peptides including having the lowest dissociation constant at 1.0×10^{-5} M [63]. HYFKFD and HFRRHL had dissociation constants of 1.1×10^{-5} M and 2.6×10^{-5} M, respectively, and Protein A had a much lower dissociation constant at 0.043×10^{-5} M [63]. Such values and orders of magnitude are consistent with other studies across the literature, and HWRGWV has repeatedly been highlighted as a peptide with promising binding performance and affinity capabilities [68].

Given the higher dissociation constants of the peptides compared to larger proteins, milder elution conditions (pH 4-6 compared to pH 3 for larger proteins) were required due to the weaker affinity which proved beneficial for minimizing the loss of product due to aggregation or denaturation [63, 67]. Proteins call for harsher elution conditions because of their higher avidity to IgG, whereas peptides enable the potential for quick and dynamic separation techniques [63]. The Fc-binding property also allows the peptide ligands to bind Fc-fusion proteins as well as orient peptides on surfaces for detection schemes [63]. Additionally, HWRGWV was the most versatile peptide in being able to bind all subclasses of IgG across a range of animal species which also played a role in its selection [63].

The HWRGWV peptide has also been characterized against bovine serum albumin to determine the nature of the peptide binding interaction to IgG [62]. When using complex medium, BSA contamination was prevalent and predicted to happen because of the unreacted groups from truncated peptide synthesis [62]. Since BSA was able to be washed off with NaCl solution, those interactions were determined to be electrostatic and non-specific in nature, whereas the peptide demonstrated more specific binding in remaining attached to the IgG [62].

SURFACE CHARACTERIZATION TECHNIQUES – the biosensor functionalization analysis of the peptide on the gold surface of the QCM utilized ellipsometry, fluorescence microscopy, SPR, and atomic force microscopy (AFM). Ellipsometry (Figure 13a) is an optical surface technique used to measure material properties of thin film interfaces [69]. The optical light source from the ellipsometer sends a stream of linearly polarized light that reflects off the QCM gold surface which changes into elliptically polarized light detected by a receiver on the opposite side [70]. The instrument has a database of surface models that are built up (quartz-titanium-gold-organic polymer layer), and the user must fit parameters to make an estimation of the thickness of

a specific layer. Fluorescence microscopy was another indicator of surface functionalization using both fluorescently tagged IgG and streptavidin. The latter used biotin as the recognition element, with the aptamer pair well known for highly selective and specific binding. Using a fluorescent microscope, absorbance and fluorescence measurements estimated the amount of analyte bound to the surface, in addition to visual observations. SPR (overviewed in Section 1.3) was also used to capture data on the surface. AFM, a technique that uses a sharp needle to mechanically probe the surface to resolve features through needle deflection (another example of MEMS described in Section 1.3) was also employed for surface characterization (Figure 13b).

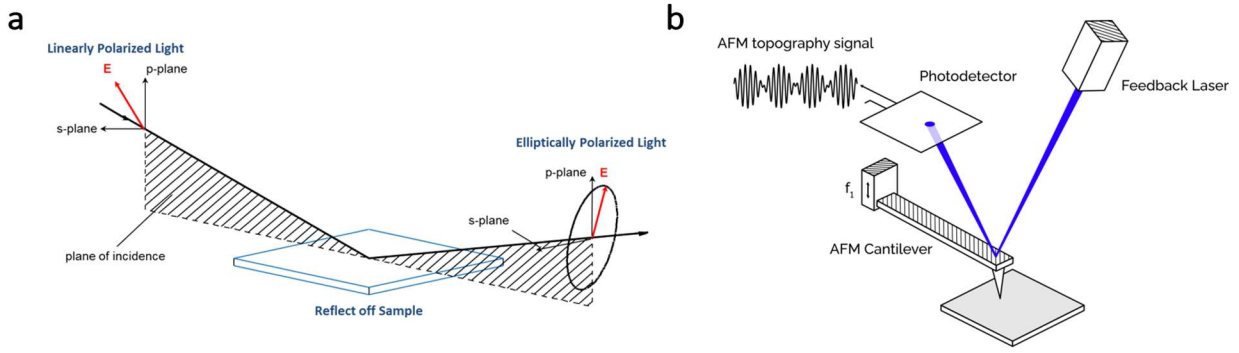

Figure 13. Examples of surface characterization techniques. (a) Ellipsometry. From J.A. Woollam [71]. (b) Atomic force microscopy (AFM). From Molecular Vista [72].

2.2 ELECTRONICS INTERFACE

Alligator clips comprised the first setup that interfaced the QCM to external electronics (Figure 14a). These were attached to the edges of the crystal where the electrodes wrap around from the top to the bottom side. However, the direct connections of the alligator clips were particularly damaging and rough on the quartz and electrode surfaces, and often made it hard to position the crystal properly due to the disorderliness of the wires. Given the exposed electronics and potential to short the circuit, introducing liquids to the QCM was difficult especially since proper operation required complete submersion of the top electrode. Before the decision was made

to design a custom printed circuit board (PCB) and microfluidics interface, another setup that was used was based on immersion (Figure 14b). This consisted of an apparatus that exposed the top electrode of the QCM and sealed the rest of the crystal with an air-tight O-ring enclosure. The immersion method was used as an initial test to observe the differences in the QCM signal between air and liquid conditions, as well as simple viscosity experiments using solutions containing glycerol and water to assess instrument and system performance.

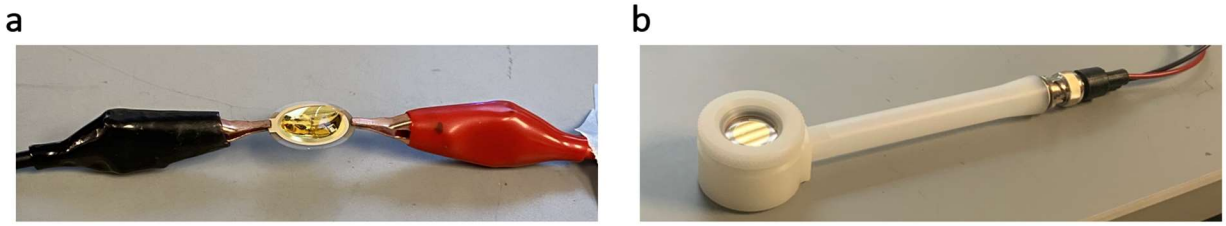

Figure 14. Initial QCM experimental setups. (a) Alligator clips attached to the top and bottom electrodes along the crystal edge. (b) QCM positioned inside of an immersion apparatus with the top electrode exposed.

Transitioning to the PCB interface allowed for more tightly controlled electronics through the incorporation of contacts and wires more conducive to radiofrequency signals. The PCB had covered traces and coaxial cables were used to connect the board to the instrumentation. Gold-finished SMA connectors and pogo pins were soldered onto the PCB to contact the QCM electrodes. The sizing of the PCB was determined by the real estate needed for the QCM, soldered components, and four screws to attach a microfluidic chamber, resulting in a board footprint that was 65 mm long and 20 mm wide (Figure 15a). Four pogo pin contacts were used under the QCM to allow for structural stability as well as enabling variability in the electrical grounding of the QCM electrodes (Figure 15b). Some examples in the literature reported that grounding the top electrode that contacts the liquid sample resulted in better signal stability [73-76]. The PCBs for the QCM were designed using EAGLE software and were ordered from OSH Park (Lake Oswego,

OR). Components were manually placed on the PCB using solder paste and tweezers, and a reflow oven was used to solidify the positioning to create a board ready for experimentation.

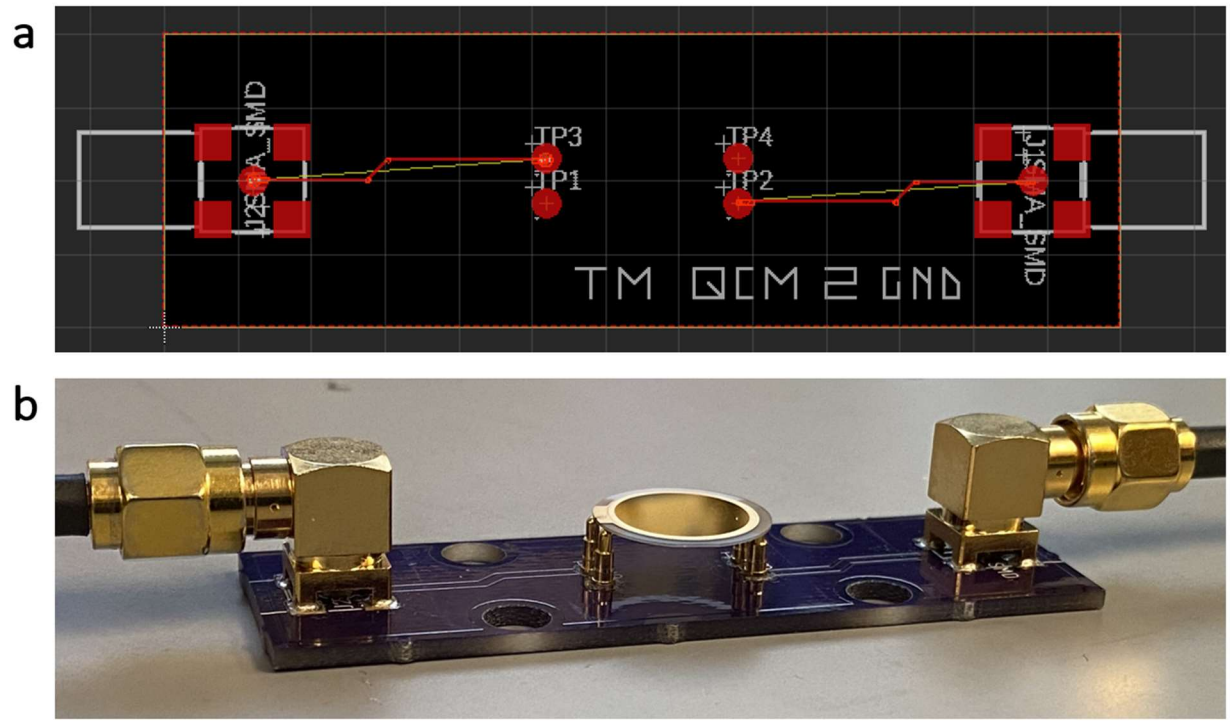

Figure 15. QCM printed circuit board (PCB) electronics interface. (a) EAGLE schematic showing the footprint of the PCB and soldered components to interface the QCM with electronics. (b) Fabricated PCB with a QCM on top of the pogo pins to demonstrate positioning.

2.3 MICROFLUIDICS INTEGRATION

The microfluidics interface enabled the introduction of liquids to the functionalized top electrode surface in a controlled manner (flow rate, volume, etc.). The design was based around the PCB and was made to enclose the QCM without adding excessive mechanical stress. The microfluidic chamber was crafted in two parts. The first part was positioned under the crystal to serve as a cradle for the QCM with a ridge to prevent the crystal from moving out of place (Figure 16a). Since the pogo pins extended vertically from the PCB and left a lot of open space (Figure 15b), it was easier to orient the QCM by placing the crystal in said cradle then shifting the crystal around to make sound electrical contact. The cradle was thick enough to ensure a slight depression

(0.5 mm) of the pogo pins. The other part of the microfluidic chamber was positioned on top of the QCM (Figure 16b) and had four characteristics: screw holes for PCB attachment, 500 µm channels for liquid flow, a cutout for an O-ring gasket to make an air-tight seal, and microfluidic tube fittings (ferrule, compression nut, Tygon tubing). Pieced together, the microfluidic chamber seamlessly integrated with the PCB and allowed the introduction of liquid samples without interfering with the electronics, while completely immersing the top functionalized gold electrode of the QCM (Figure 16c). The microfluidic chamber was initially developed using 3D-printing techniques, but the resolution of the features was too poor to be functional for experiments. CNC machining proved to be more effective, and acrylic was used as the material for the microfluidic chamber due to its biocompatible properties as well as its transparency to visualize the liquid flow. Two iterations of the microfluidic chamber were made, with the second one modified for better stability of inner components and increasing the height of the top part of the chamber to accommodate the tubing components at the inlet and outlet. The microfluidic chambers were custom designed in Fusion 360 and ordered from Xometry (Gaithersburg, MD).

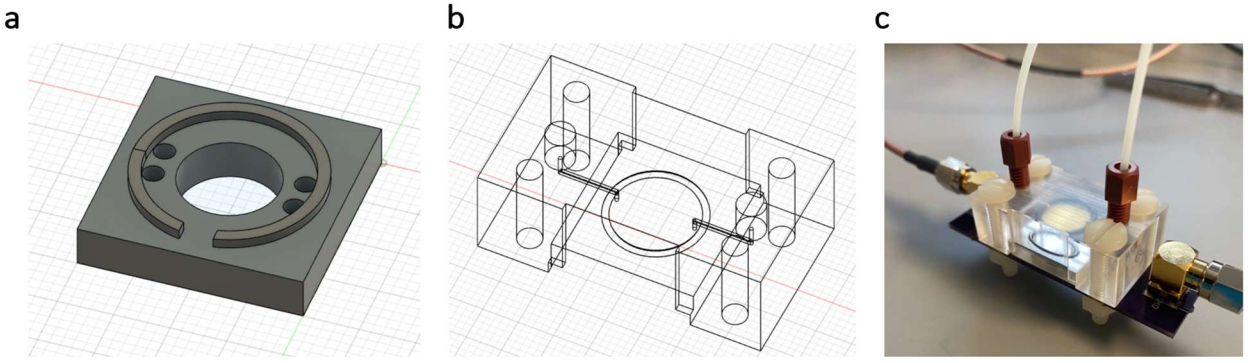

Figure 16. QCM microfluidic chamber to interface biosensor with liquids. (a) QCM cradle to orient the crystal on top of the pogo pins. (b) QCM enclosure including the microfluidic channels, screw holes, and gasket cutout. (c) Microfluidic chamber parts pieced together on the PCB.

Most experiments in this body of work used a syringe pump to introduce liquids to the QCM. A syringe was connected to the Tygon tubing at the inlet, and an outlet tube dumped waste

into an open beaker. To prevent the appearance of air bubbles, the biosensor was positioned vertically during initial flow and then taped down horizontally to the benchtop to prevent any further physical or mechanical shifts to the system from handling or changing syringes. PBS was first introduced to the QCM as a buffer to equilibrate the system to acclimate the surface to a liquid environment. Once the system stabilized as determined by negligible changes in the signal response, the PBS syringe was carefully swapped with another syringe containing a sample of a concentration of IgG or other analyte in PBS. All solutions were typically flowed at a rate of 30 μL/min, and to prevent material waste, experiments were planned to run only 30 minutes of IgG solution. After every IgG sample, the QCM was washed by flowing PBS to remove excess IgG that did not bind to the surface. The peak frequency of the QCM after this final PBS wash step was subtracted from the peak frequency prior to the sample after initial equilibrium to determine the shift in resonant frequency due to mass loading. Experiments with consecutive concentrations of IgG utilized a PBS washing step before and after every sample of analyte.

2.3.1 INFLUENCE OF SYSTEM PRESSURE

The resonant frequency of the QCM is affected by mass loading, surrounding fluid properties (viscosity and density), adsorption on the surface, temperature, surface roughness, and pressure [77]. Pressure gradients and viscous drag over the surface of the crystal change the behavior of the signal, and fluctuations in pressure negatively impact the overall response [47, 78, 79]. The introduction of fluid flow adds a dynamic component that certain systems account for in resolving the signal [47]. Typically, thicker crystals (5-10 MHz) are employed across the literature due to their resilience against pressure differences compared to the thinner, higher frequency, and more sensitive crystals [47]. In addition, slow flow rates or large cell flow volumes have also been used to combat these challenges [47]. In one scenario, it was shown that pressure surges from a

pump at high flow rates fluctuate the signal and may cause the frequency to shift [79]. It was determined that the total frequency shift was made up of a mass deposition component and a hydrostatic pressure component, since the emergence of pressure can deflect the QCM [79]. Hydrostatic pressure increases at higher flow rates, thus the resonant frequency may shift accordingly with increasing flow rate as shown in Figure 17 [79].

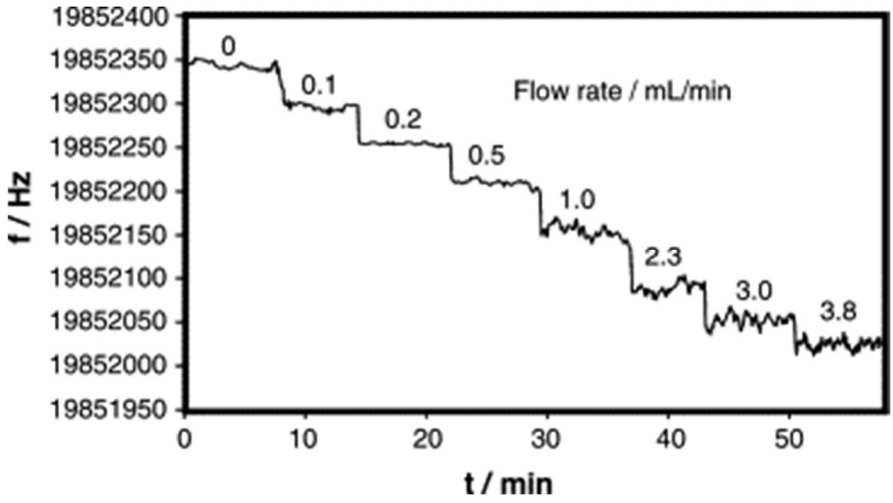

Figure 17. Impact of flow rate on QCM frequency response. Increasing the flow rate results in a shift in frequency and less stable signals. From Michalzik *et al* 2005 *Sensors and Actuators B: Chemical*, reprinted with permission from Elsevier [79].

Increasing the flow rate adds an apparent mass loading to the system, and using fluids with higher viscosities or rough crystal surfaces would result in more drastic impacts due to more viscous drag [78]. Others have shown how pressure proportionally increases the frequency exhibited by the QCM [80, 81]. The hydrostatic pressure may also have an impact on the adsorption and desorption of particles, which is particularly problematic for the truly accurate detection needed in biomedical and bioprocess applications [78, 82].

With regards to clamping the microfluidic chamber housing to the PCB, this creates a damping influence on the QCM [83]. The pressure exerted on the QCM from the system may make the crystal more susceptible to the negative impact of hydrostatic pressure and viscous forces [83].

It was also noted that it may be advantageous to utilize a QCM setup that is totally immersed (both electrodes) in a non-conductive liquid with a low dielectric constant to create a more uniform and distributed profile to prevent asymmetric forces from acting on the crystal [83, 84].

The prevalence of back pressure may also contribute to various problems, and this was likely seen in the QCM biosensor system from time to time. One issue may have been the tube length of the inlet and outlet, which should be standardized as to not increase flow resistance over the active detection area [85, 86]. Also, when syringes were switched between samples in experiments, that also caused significant changes in pressure exerted on the QCM. Furthermore, the waste tube was placed over a beaker without constant volume, and the waste droplet that was formed before falling off most likely caused perturbations in system pressure. Even though the outlet tube was positioned along the side of the waste beaker, the formation and subsequent release of droplets into the reservoir added a fluctuation of pressure across the system. The analysis of pressure contributions was performed retroactively and would be incorporated into future iterations of the QCM biosensor system design.

2.4 EXPERIMENTAL INSTRUMENTATION

The tools used for conducting QCM experiments served the purpose of extracting the resonant frequency of the biosensor and enhancing the analysis of results. A variety of hardware and software were used during experiments to characterize biosensor operation and system performance. Although many of these instruments are expensive and counterintuitive for a setup that needs to be accessible, the first step toward realizing that goal is a thorough assessment of the biological phenomena on the surface as well as the physics behind QCM operation given the biosensor device and design at hand.

2.4.1 HARDWARE

VECTOR NETWORK ANALYZER – A Tektronix TTR500 vector network analyzer (VNA) was used for initial QCM experiments to determine the location and characteristics of the resonant frequency peak via the scattering parameters of the system (Figure 18). Specifically, the S11 (reflection) and S21 (transmission) parameters were used to draw conclusions. The VNA drives a voltage through the circuit and detects the signal that gets bounced back from the QCM to the source (S11) and the signal that transmits through the QCM into the receiving port of the VNA (S21). These parameters provide information needed to characterize the behavior of radiofrequency signals and system performance. The plots produced by the VNA have frequency on the x-axis measured in hertz (Hz), and power on the y-axis measured in decibels (dB). Many initial tests were general observations regarding the shape and shifts of both the frequency and amplitude of the resonant frequency peak of the QCM.

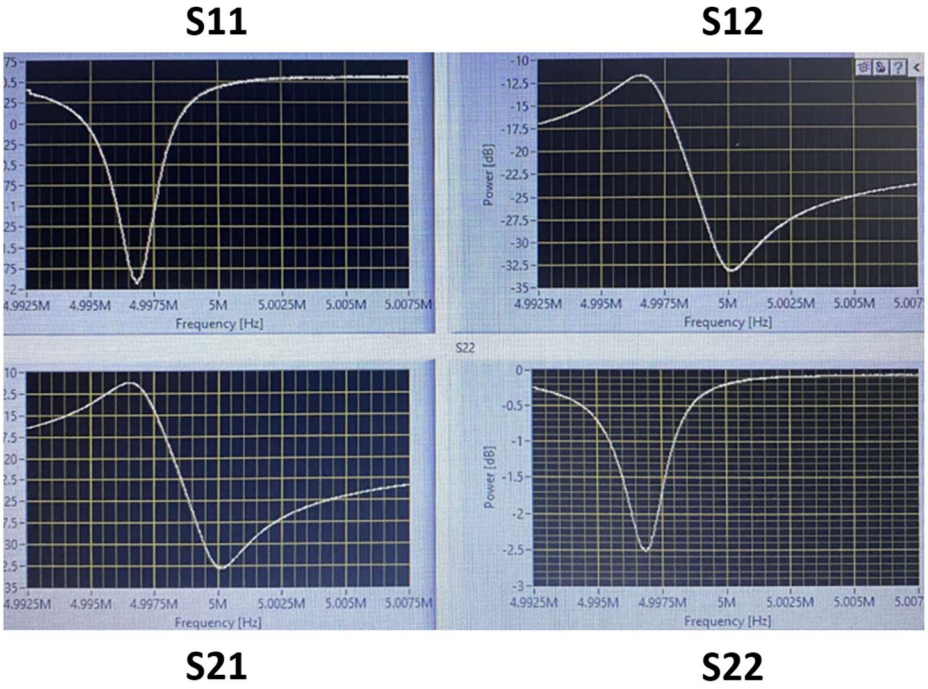

Figure 18. VNA scattering parameter output of 5 MHz QCM in air. S11 and S21 are frequently used parameters for QCM measurements across the literature.

MULTIPLEXER – A Pickering RF Multiplexer was used to connect the VNA to the device under test (DUT) which in this case was the QCM biosensor system. The available instrument configuration could allow for measuring sixteen QCM biosensors at the same time, crucial for exploring the capabilities of arrayed detection. The coaxial cable extended from the PCB and connected to SMA sockets on the multiplexer, continuing the connection to the VNA or lock-in amplifier which sourced the signals and generated the data for analysis.

LOCK-IN AMPLIFIER – A Zurich Instruments HF2LI 50 MHz Lock-in Amplifier was used as a more advanced signal generator and analyzer, given its higher resolution and more options for tuning the sampling parameters for sweeping the frequency range in resolving the resonant frequency peak. Furthermore, this instrument made it possible to detect the resonance overtones, which are key in some viscoelastic models to characterize QCM systems. Transitioning to this instrument was influenced in part by the difficulty in controlling the stability of the QCM signal. The lock-in amplifier allowed for phase-locked loop (PLL) detection that took the phase of the signal into account rather than just the location of the peak. Phase itself is a comparison between a reference signal and an input signal, with differences tracked and compared over time [87]. The resonance of a biosensor system can shift for any number of reasons external to binding on the surface, but changes in the environment or crystal itself have an impact such as touching the biosensor device, which was difficult to manage when swapping syringes during experiments. The PLL would intrinsically capture the environmental and surface conditions which eliminated some noise and variability in the analysis of the signal.

FARADAY CAGE – The Faraday cage is a tool used to reduce the effects of external electromagnetic radiation (i.e. electronic noise) [88]. A wooden frame was wrapped with a copper mesh screen (Figure 19a), and this was one of the many techniques employed to try to further

understand abnormal signal behavior of the resonant peak under static and flowing conditions. A cardboard box covered in aluminum foil constituted another attempt at a Faraday cage to address issues in signal stability (Figure 19b-c).

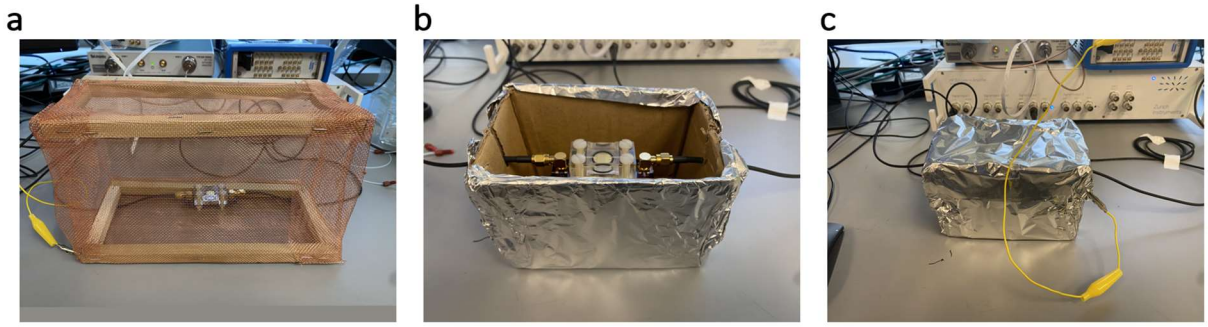

Figure 19. Faraday cage setups used for the QCM biosensor. (a) Copper mesh screen surrounded by a wooden frame. (b) Open cardboard box encased in thick aluminum foil. (c) Closed cardboard box surrounded by aluminum foil.

2.4.2 SOFTWARE

LABVIEW – LabVIEW is an automation software with a customizable user interface that was used to run QCM experiments by controlling the timing and operational parameters of the VNA and multiplexer. The software could also be programmed to output .csv files and graphs in formats that allowed for easier visualization and data analysis. The lock-in amplifier had its own environment for running experiments and outputting data, although the instrument included the software drivers to connect to LabVIEW software. However, the setup to connect the lock-in amplifier to LabVIEW was less straightforward, so LabVIEW was used for initial QCM experiments with the VNA. The experimental setup of the block diagram and front panel can be found in Appendix A.

MATLAB – The numerical programming environment in MATLAB was often the last step in processing QCM data and making any calculations or polished plots. Files from the VNA or lock-in amplifier were imported into MATLAB for plotting the resonant frequency, resonant

frequency shift, resonant frequency amplitude, resonant frequency amplitude shift, and other theoretical measurements to describe the behavior and performance of the QCM biosensor system. The base code can be found in Appendix B.

COMSOL – The powerful multiphysics simulation software in COMSOL was used to model the QCM and the mechanical shearing of the crystal under stress as a piezoelectric material connected to a live circuit. Attempts were made to add organic matter and mass loads to the surface with limited success. Utilizing COMSOL would be a crucial first step for designing an arrayed QCM setup to estimate the signal response and interactions between adjacent electrodes.

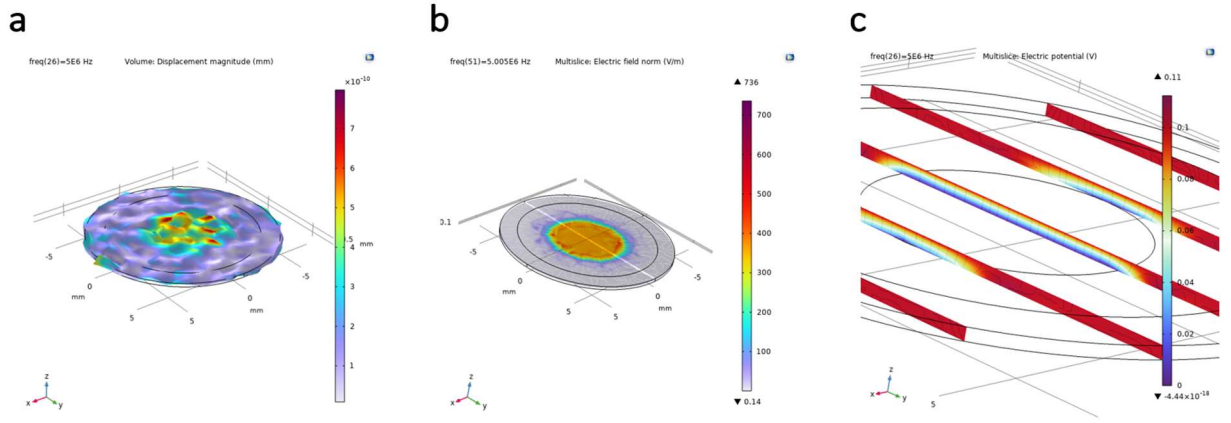

Figure 20. COMSOL models of the QCM biosensor. (a) Volume displacement showing the shearing of the quartz at the overlap between the top and bottom electrodes. (b) Electric field showing the most activity where the top and bottom electrodes overlap. (c) Electric potential decreasing at further distances from the top electrode surface.

The images in Figure 20 were created with the assistance of the Thickness Shear Mode Quartz Oscillator tutorial provided by COMSOL, starting by using the "Piezoelectricity, Solid" model in the "Structural Mechanics" physics tree with quartz as the material [89]. The oscillator radius was 6.975 mm and the thickness was 270 µm. The top electrode had a radius of 5.6 mm and the bottom electrode was 2.8 mm, both with thicknesses of 200 nm. The gold electrode layers were connected used the "Electrostatics" modeling in the software with the top and bottom acting as terminal boundary conditions. The applied voltage ranged anywhere between 100 mV and 10 V,

as these were the available input settings on the lock-in amplifier. These models were coupled together and integrated to produce the graphs for shear displacement, electric field, and electrical potential (Figure 20) with the plotting tools in the modeling software.

3. EXPERIMENTAL RESULTS

3.1 SURFACE CHARACTERIZATION

The thickness of the peptide recognition element layer on the functionalized electrode surface was analyzed using ellipsometry. Optical constants for gold as the reference substrate were $N_s = 0.17492$ (refractive index) and $K_s = -4.2874$ (extinction coefficient). A peptide thickness of 180 angstroms was used as an estimation, but after biosensor functionalization, the ellipsometer measured the peptide layer to be 12.86 angstroms which was off by an order of magnitude. However, this still indicated that something was bound to the surface, and the discrepancy may have been a result of the negative extinction coefficient or a non-uniform spatial arrangement of peptide within the ellipsometer sampling region on the electrode (measurements are the average of detected heights). To ensure the ellipsometer was running properly, wet thermal oxide silicon blanks were tested with known thicknesses of 50 nm and 200 nm. Optical constants for a 0 nm thickness silicon blank as the reference substrate were measured at $N_s = 3.8827$ and $K_s = 0.019626$. The 50 nm thermal oxide measured at 387.55 angstroms thick compared to an expected 500 angstroms, and the 200 nm thermal oxide measured at 2,236.74 angstroms compared to an expected 2,000 angstroms. Across wavelengths, thicker layers resulted in more accurate measurements, so the estimated low thickness of the functionalized peptide layer may have also contributed to the unexpected result.

Fluorescence and absorbance were additional measures for surface functionalization validation using 20 µg of fluorescently tagged streptavidin. After flowing the streptavidin sample over the QCM, the frequency shift was 30 Hz. Calculations determined that 16.86 µg of streptavidin loaded onto the surface based on absorbance measurements, and 2.44 µg based on fluorescence. Two experiments were conducted using fluorescently tagged IgG, with

concentrations of 100 µg/mL and 200 µg/mL (Figure 21). The 100 µg/mL IgG sample saturated after approximately 30 minutes, capturing 10.64 µg (based on fluorescence) out of the 100 µg of IgG exposed to the surface in the 1 mL volume sample (~10% capture efficiency). The 200 µg/mL IgG sample also saturated after approximately 30 minutes, but captured 19.10 µg (~10% capture efficiency once again). These fluorescence experiments in particular both happened to result in total frequency shifts of 30 Hz.

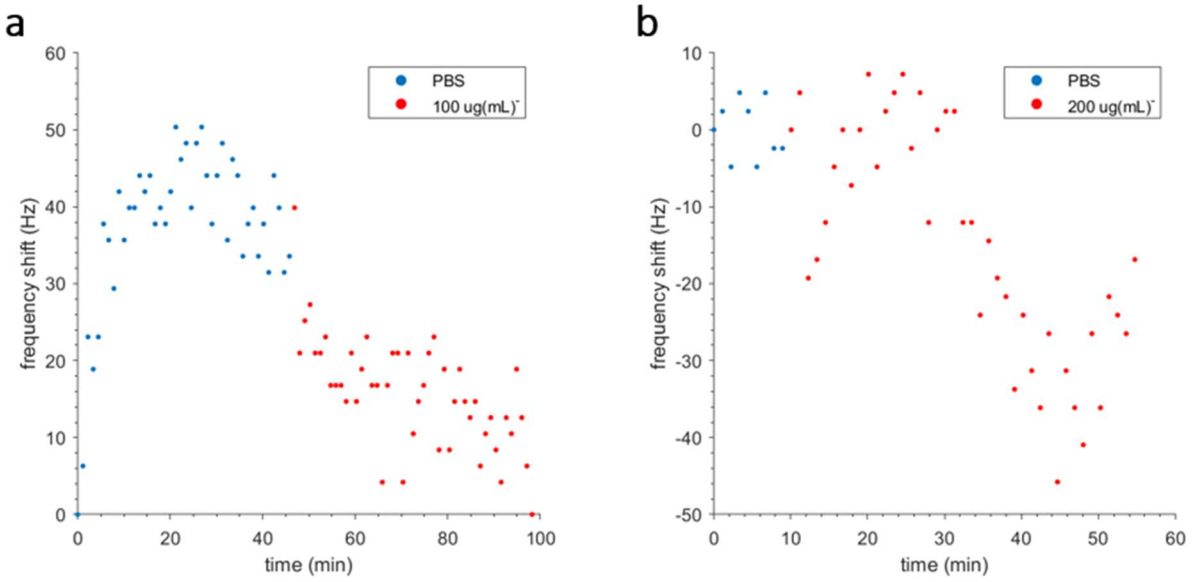

Figure 21. QCM binding experiments utilizing fluorescent IgG. (a) 100 µg/mL experiment captured 10.64 µg of analyte. (b) 200 µg/mL experiment captured 19.10 µg of analyte.

AFM measurements were also captured using the parameters outlined in Figure 22. Topological changes of the surface after each functionalization step indicated the formation of the SAM complex. SPR data (Figure 23) highlighted the dose-dependent curves based on varying concentrations of IgG diluted from stock, and showed specificity toward IgG against bovine serum albumin (BSA) and human serum albumin (HSA) proteins. This provided further validation of the surface chemistry schema designed for the QCM biosensor.

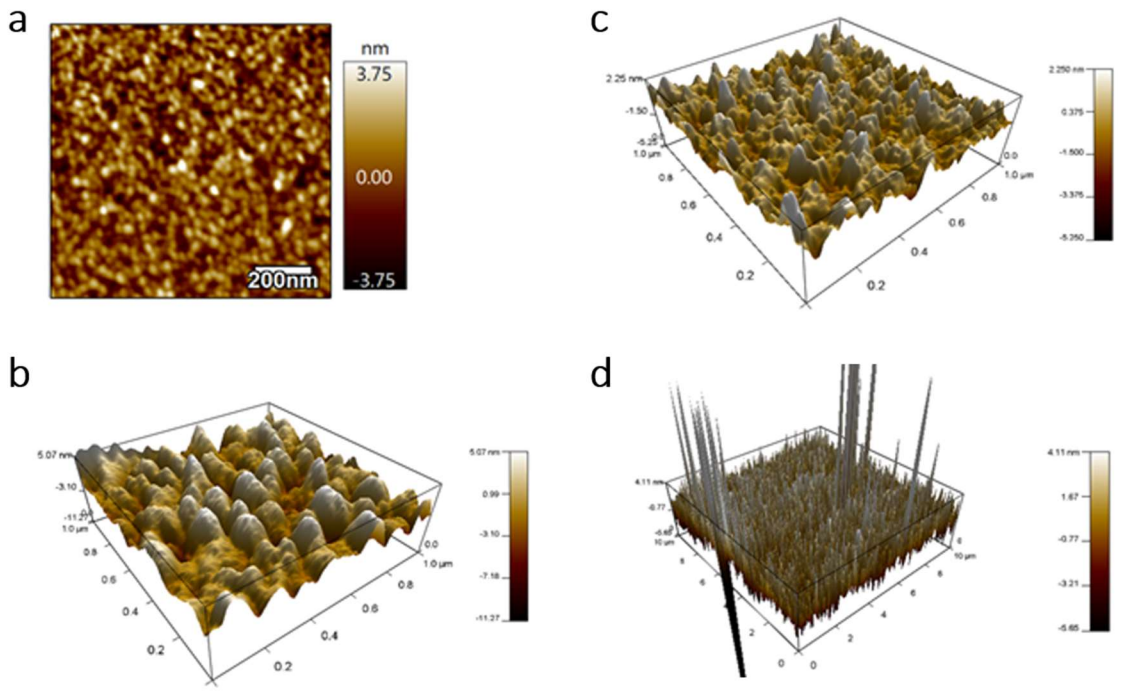

Figure 22. Atomic force microscopy (AFM) measurements of blank gold wafer and functionalized QCM. Local structural analysis of SAM on gold surfaces to determine characteristics upon each functionalization step using the following parameters: Imaging mode: AC mode. Scan lines: 256. Scan points: 256. Scan rate: 0.75 Hz. Scan size: 1.00 µm / 10.00 µm. (a) Surface roughness of blank gold wafer. (b) Topology of blank gold wafer incubated in PBS buffer. (c) Topology of QCM incubated in PBS buffer. (d) Topology of QCM incubated with peptide complex in PBS buffer. Courtesy of Dr. BangHyun Lee, BioInterface Lab.

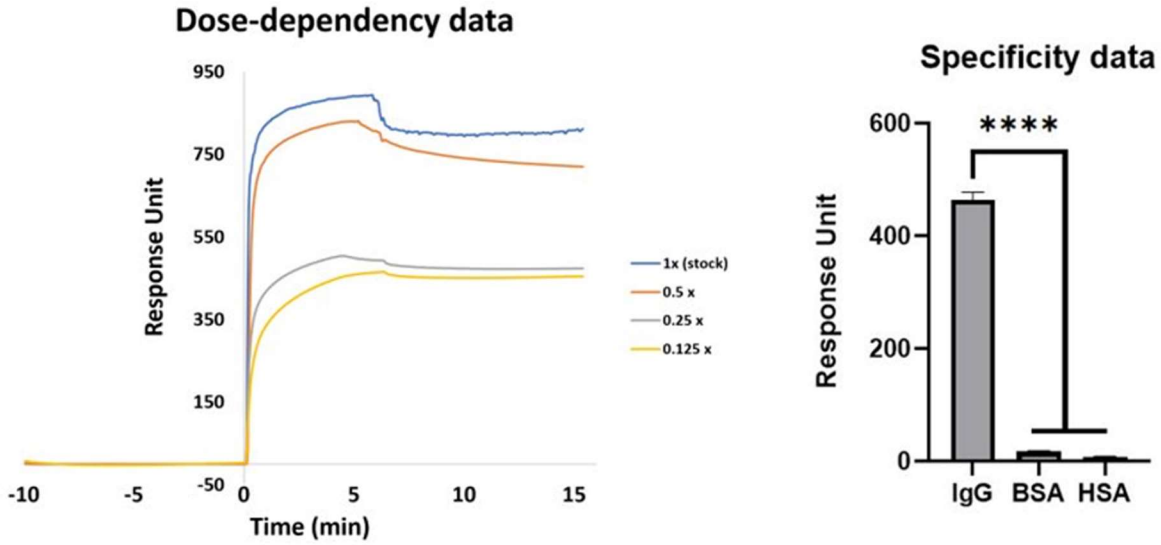

Figure 23. Surface plasmon resonance (SPR) measurements of peptide functionalization. Dose-dependency and specificity data to validate and characterize the surface functionalization used for the QCM biosensor. Courtesy of Dr. BangHyun Lee, BioInterface Lab.

3.2 INITIAL QCM TESTING

The difference between QCM operation in liquid versus air was very profound. A decrease in the resonant frequency peak amplitude, broadening of the resonant frequency peak (reduction of Q factor), and shift in resonant frequency due to viscoelastic loading can be seen in Figure 24. Switching between air and PBS resulted in reproducible shifts of approximately 800 Hz. Many QCM whitepapers model baseline performance through viscosity measurements using various mixtures of glycerol in water. The behavior of the QCM across 5-25% glycerol samples shown in Figure 25 exhibited great correlation to theoretical estimations [90].

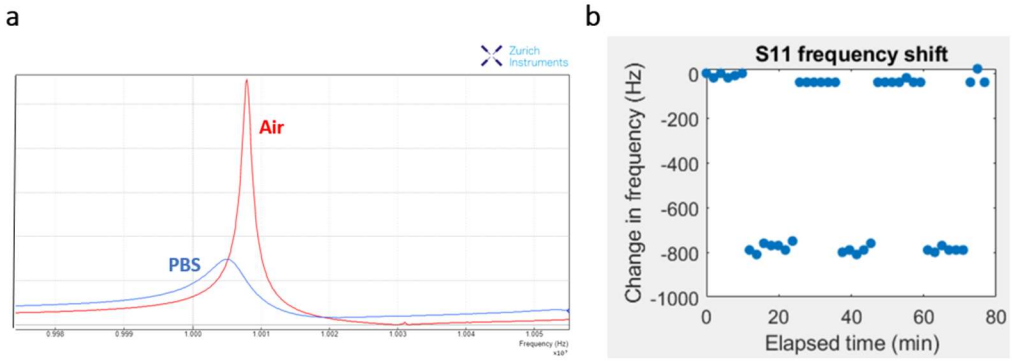

Figure 24. QCM frequency response in air vs. PBS. (a) Switching between air and PBS drastically reduced the Q factor and shifted the resonant frequency peak to the left. (b) Switching between air and liquid conditions produced 800 Hz shifts in the resonant frequency.

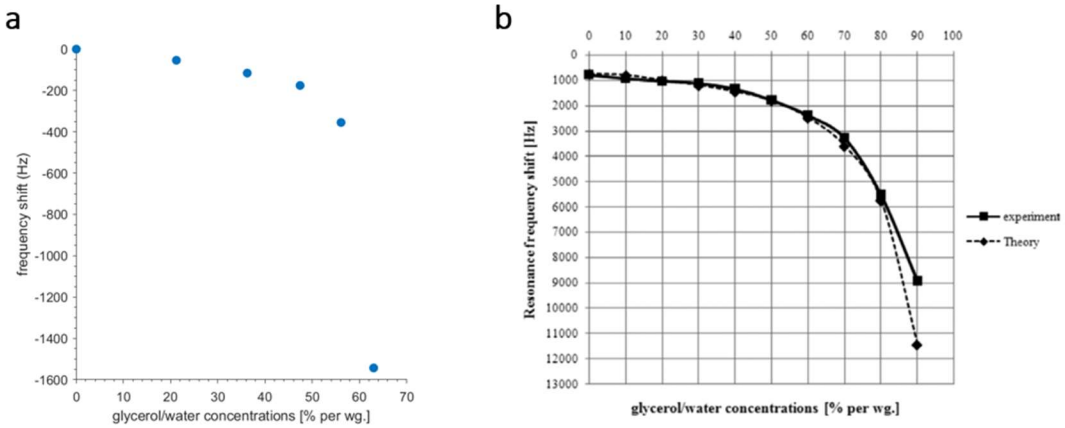

Figure 25. QCM viscosity measurements of glycerol-water mixtures. (a) Experimental measurements of the QCM as a viscosity sensor. (b) Experimental vs. theoretical QCM frequency response viscosity results. From Esmeryan *et al* 2013 *J. Phys. D: Appl. Phys.*, reproduced with permission from IOP Publishing [90].

3.3 QCM BINDING STUDIES

The ability of the QCM to detect IgG was the ultimate determinant of the efficacy of the biosensor design. The aforementioned fluorescence experiments served as surface functionalization validation, but also showed the capability of the biosensor system to bind IgG. The proper bounds of IgG concentrations to use in experiments had to be determined by figuring out the dynamic range of operation. This range can be impacted by the integrity of the recognition element or spatial density of binding sites. Initial experiments typically portrayed negligible variance in response at concentrations lower than 10 µg/mL and higher than 1-2 mg/mL, so the dynamic range was determined to be between 10 µg/mL and 1 mg/mL. This range can be seen in Figure 26, where increasing concentrations of IgG were consecutively flowed over the QCM depicting a distinct response profile between the two bounds.

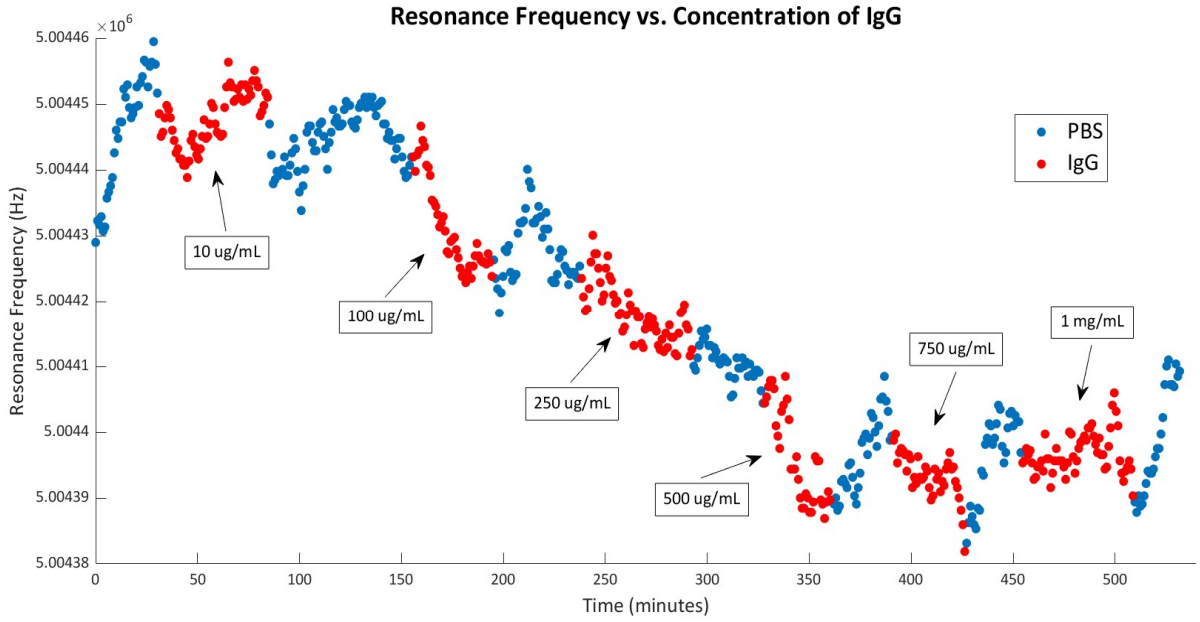

Figure 26. QCM binding experiment with consecutively increasing concentrations of IgG. The dynamic range was established by determining the limit of detection and saturation limit.

This experiment resulted in a saturation frequency difference of approximately 80 Hz, further highlighting the limited resolution that can arise for biosensor operation in liquids. Another

experiment utilized a single concentration of IgG as shown in Figure 27, and the impact of the IgG being introduced to the system was immediately observable on both the amplitude and frequency responses.

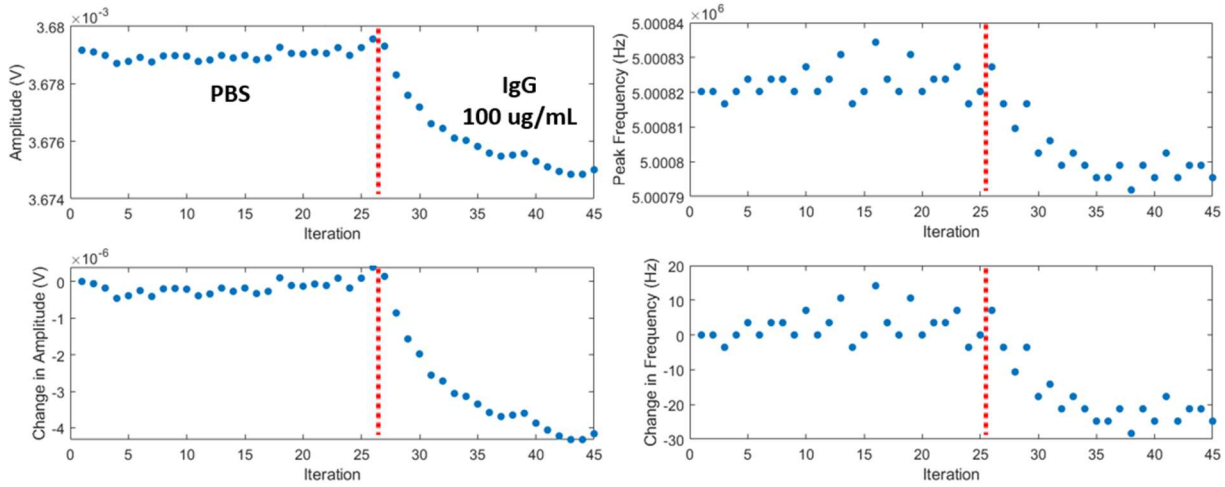

Figure 27. QCM amplitude and frequency responses after introduction of IgG. The QCM biosensor system immediately responded to the introduction of 100 µg/mL of IgG. Each iteration is 1 minute.

The tests herein demonstrate that the QCM biosensor had the capability to detect a range of IgG analyte concentrations. Figure 28 used 500 µg/mL of IgG and Figure 29 used 1 mg/mL of IgG. The response behavior in Figure 28 showed a rapid decrease in resonant frequency as opposed to the prolonged decrease as seen in Figure 29, and such variance was expected with a custom biosensor. However, optimal results would portray identical magnitude shifts in frequency at saturation, and the higher concentrations of analyte would achieve saturation faster which is the opposite behavior shown across Figure 28 and Figure 29.

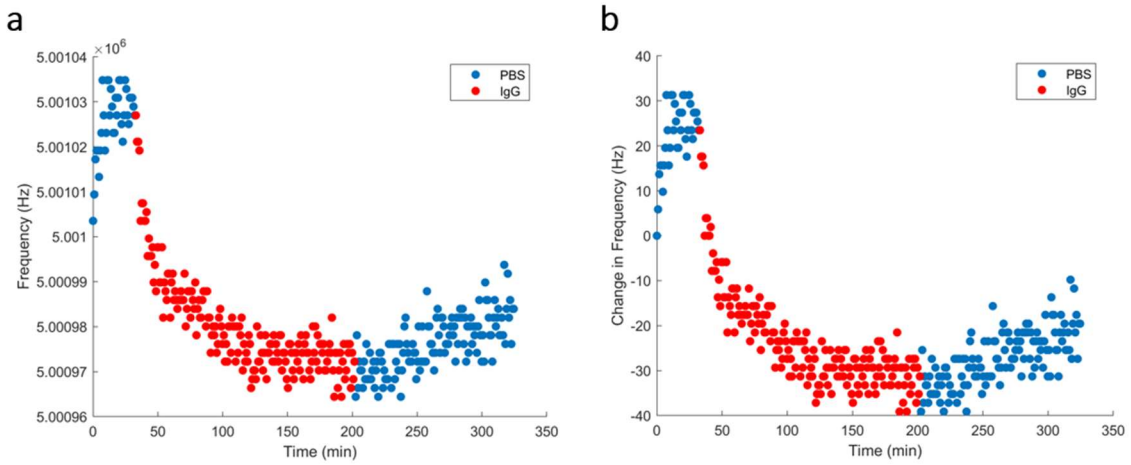

Figure 28. QCM binding experiment utilizing 500 µg/mL of IgG. (a) Frequency response. (b) Frequency shift showing a 50 Hz decrease.

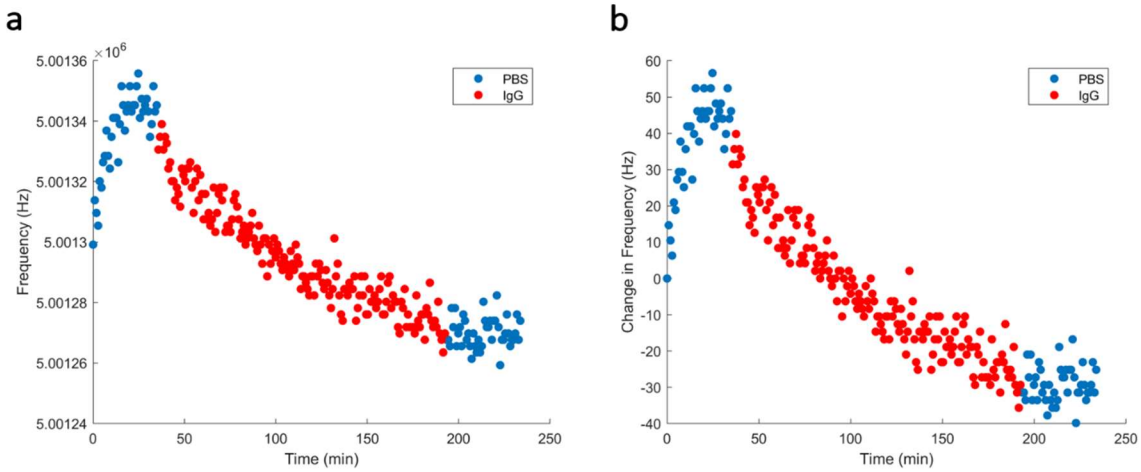

Figure 29. QCM binding experiment utilizing 1mg/mL of IgG. (a) Frequency response. (b) Frequency shift showing a 75 Hz decrease.

However, binding rate dependency on concentration was seen in a different set of experiments using 100 µg/mL, 500 µg/mL, 750 µg/mL, and 1 mg/mL of IgG (Figure 30).

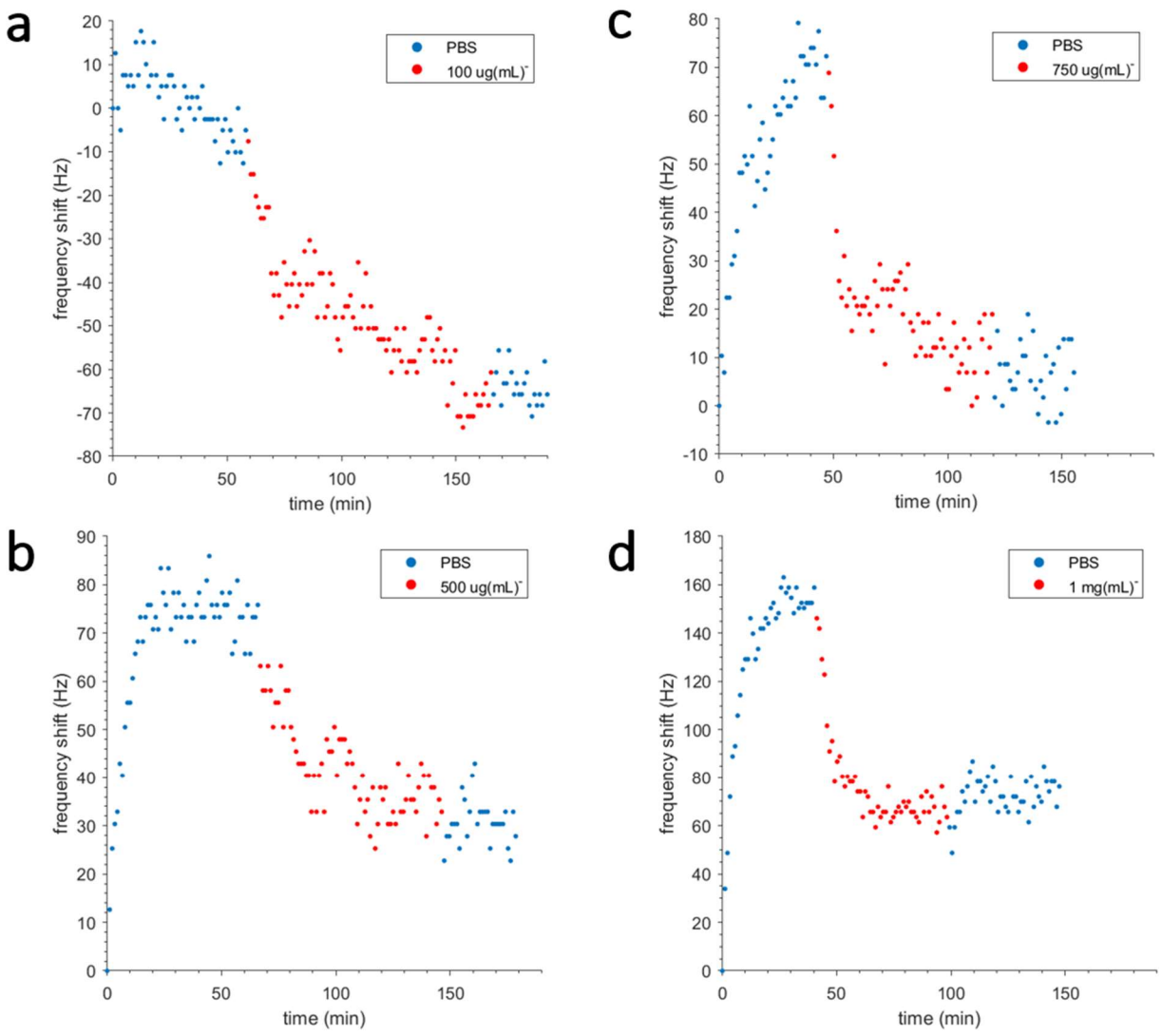

Figure 30. Binding rate dependency on IgG concentration. (a) 100 µg/mL resulted in a frequency shift of 70 Hz. (b) 500 µg/mL resulted in a frequency shift of 45 Hz. (c) 750 µg/mL resulted in a frequency shift of 60 Hz. (d) 1 mg/mL resulted in a frequency shift of 75 Hz.

These experiments focused on using one concentration of IgG per QCM biosensor, as opposed to the consecutive concentrations for the dynamic range in Figure 26. Once the baseline stabilized in PBS, the goal was to flow a concentration of IgG as long as necessary for the signal to saturate before washing with PBS as the final step. In Figure 31, the binding rate dependency across concentrations highlights the potential of time to saturation as a metric for determining analyte concentration.

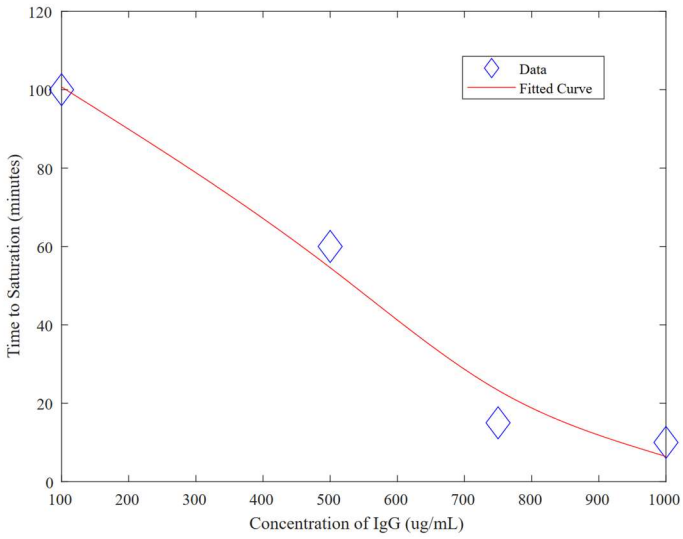

Figure 31. Time to saturation across concentrations of IgG.

In another set of experiments, two concentrations of streptavidin were used as shown in Figure 32. The frequency response profiles showed resemblance to one another, although complete saturation was not able to be observed due to limits on the amount streptavidin available to use. However, both tests resulted in a decrease of 30 Hz given the amount of streptavidin that was exposed to the surface over the course of approximately 1 hour. The streptavidin experiments were used as an extra measure to verify signal response with a known binding pair.

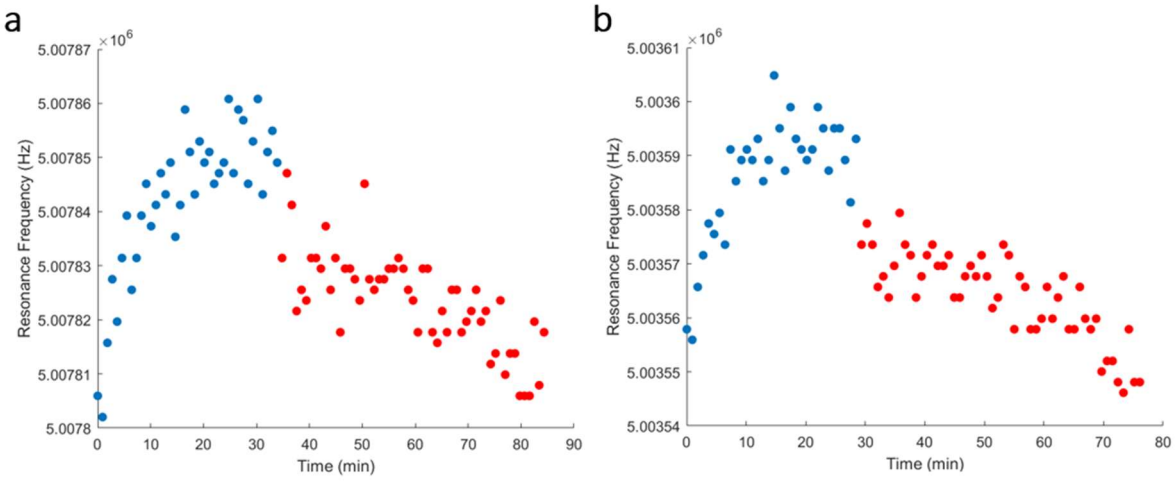

Figure 32. QCM binding experiments utilizing streptavidin. (a) 100 µg/mL of streptavidin (red) after PBS (blue). (b) 200 µg/mL of streptavidin (red) after PBS (blue). Both experiments resulted in a 30 Hz decrease in frequency.

3.4 QCM STABILITY TESTS

Making use of the PLL for IgG binding experiments was intended to solve the problem of response inversion and oscillatory behavior in the frequency response, but due to the makeshift biosensor design and experimental setup, certain tradeoffs were deemed acceptable for signal quality and stability. One prevalent observation was the relationship between the amplitude and the frequency response. In Figure 33, the amplitude and frequency initially increase in tandem, but only when the amplitude stabilized was the expected frequency behavior seen.

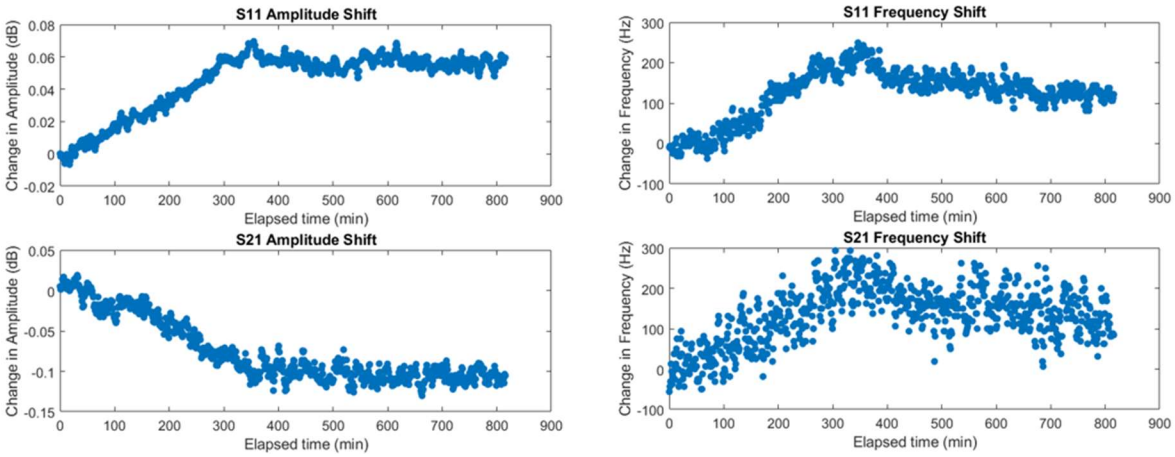

Figure 33. QCM baseline drift experiment in PBS. The QCM biosensor ran overnight in PBS to determine baseline drift. It was clear that the amplitude needed to stabilize before any accurate measurement of frequency response could be made.

In other examples, when the amplitude increased and stabilized, the frequency shift had a stable but inverted response in the opposite direction (Figure 34). These abnormalities could not be explained but such behavior has been noted across the literature, with one source attributing the phenomena to non-uniform mass distribution on the surface and another source claiming this happens when the coupled layer has high viscous dissipation of energy and is relatively thick as portrayed in Figure 35 [38, 91, 92].

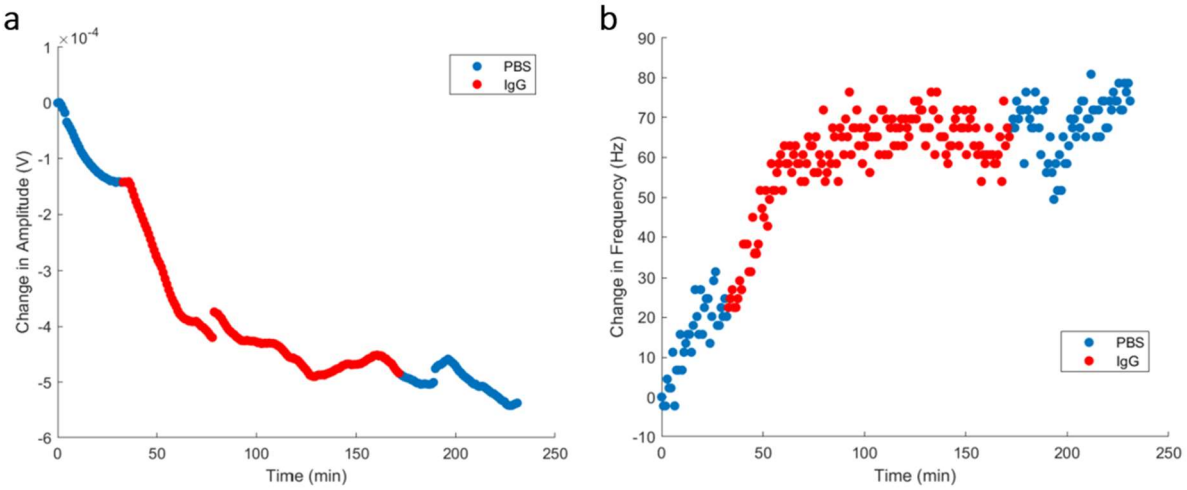

Figure 34. Inverted frequency response behavior during IgG binding experiment. Concentration used was 100 µg/mL. (a) Amplitude shift. (b) Introduction of IgG shows an increase in resonant frequency rather than a decrease.

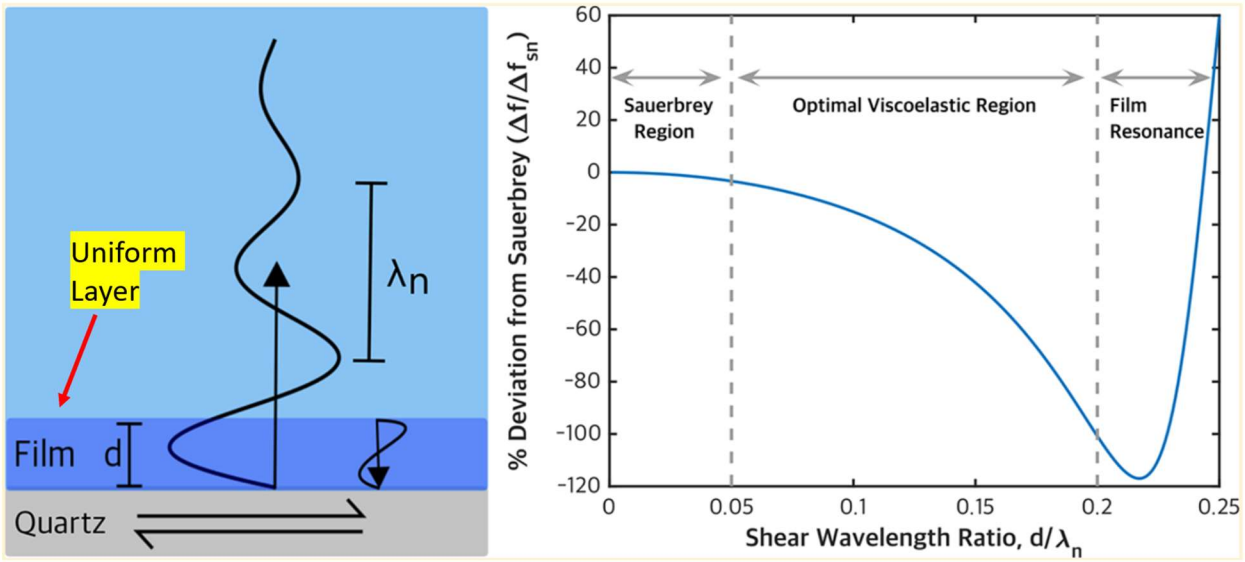

Figure 35. Model of film thickness as a ratio to expected resonance behavior. Deviations from the Sauerbrey equation (Equation 1) depend on film thickness and penetration depth. A hydrogel film was used in this example which ensured uniformity in mass distribution across the QCM which were ideal conditions. Adapted from Sadman *et al* 2018 *Anal. Chem.*, with permission from the American Chemical Society [92].

In Figure 36, the oscillatory behavior of the response was predicted to be caused by external electromagnetic interference. To prevent this behavior, it was very important to carefully handle the biosensor system and ensure that everything remained as unchanged as possible during

experiments. Methods such as taping down the wires or exploring the use of a more hands-off microfluidic control system set out to address these issues in stability. The syringe pump was the nearest piece of metal to the biosensor, but the oscillatory response persisted even with its removal.

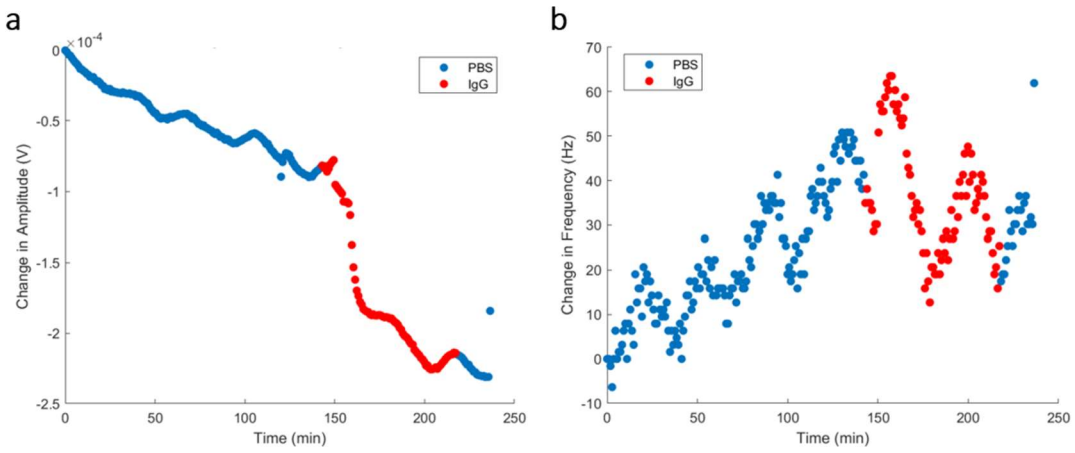

Figure 36. Oscillatory frequency response behavior during IgG binding experiment. The concentration used was 1 mg/mL. (a) Amplitude shift. (b) Periodic oscillations in the frequency response.

Figure 37 used 500 µg/mL of IgG and showed an increasing frequency response similar to Figure 34 as well as the oscillatory behavior seen in Figure 36. Figure 38 evaluated the frequency response in PBS with oscillations prevalent in both the amplitude and frequency response signals. One important consideration to note is that the experimental setup for the biosensor system lacked temperature control, which is often a critical component of signal stability.

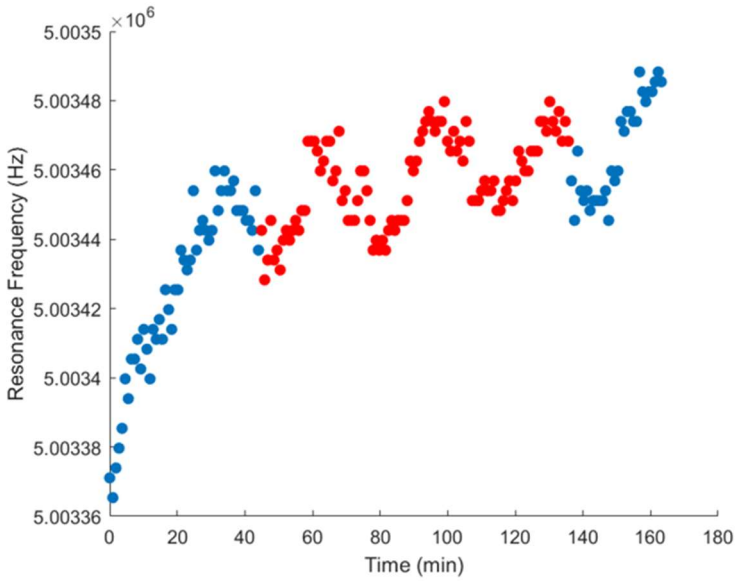

Figure 37. Oscillatory and increasing frequency response behavior during IgG binding experiment. Concentration used was 500 µg/mL of IgG (red) between PBS flow (blue).

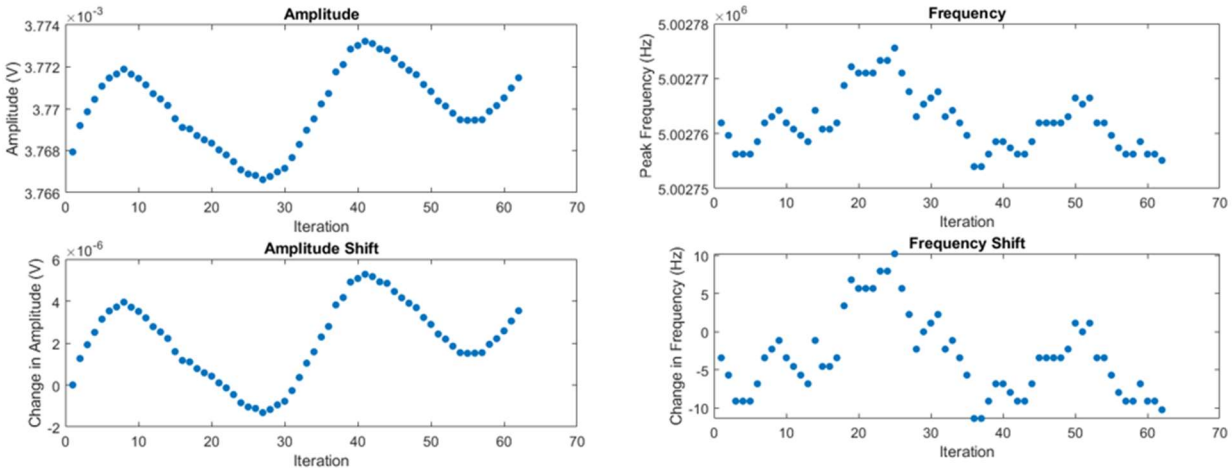

Figure 38. Oscillatory frequency response behavior in PBS. Each iteration is 1 minute.

The PLL locks on to the phase conditions of the biosensor to provide a truer depiction of the resonant frequency of the system. Options for setup included denoting parameters for PI or PID control loops, which required a deep understanding of the system at hand for proper tuning. Given that the instrumentation was being used to acquire said deeper understanding, there was a chicken and the egg problem due to the PLL parameters being needed for accurate measurements, but accurate measurements being needed to fine tune the parameters. This could be one of the

various reasons why the expected responses were not seen over the course of the PLL experiments. The test in Figure 39 to establish a baseline in PBS highlights such unpredictability of the response.

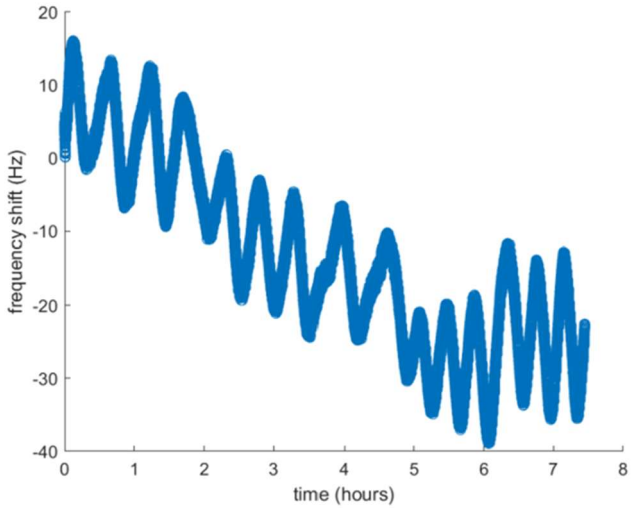

Figure 39. Oscillatory frequency response behavior in PBS using the PLL. Baseline had difficulty establishing over several hours, and the oscillatory behavior continued to be seen in a handful of experiments.

The addition of the Faraday cage proved negligible toward signal stability of the biosensor system (Figure 40b), so the conclusion was to ensure more tightly controlled environmental conditions given the periodicity of the oscillations.

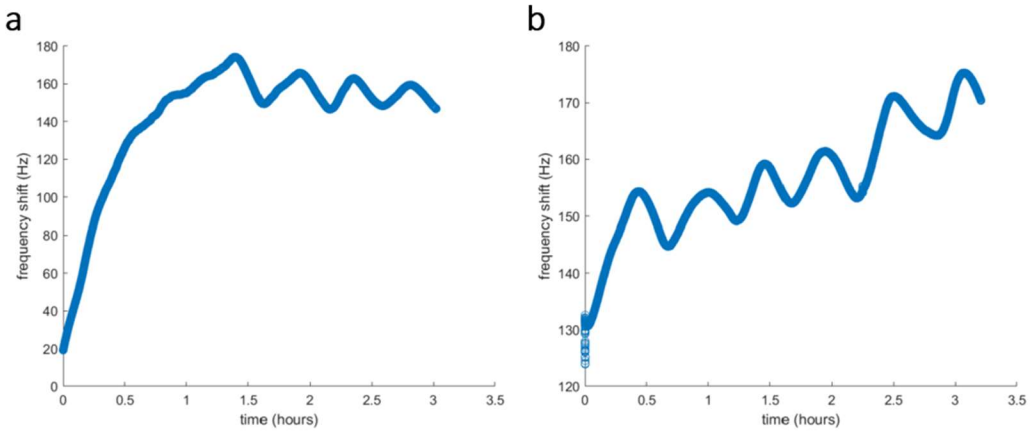

Figure 40. Frequency response in PBS using a Faraday cage. (a) Frequency response without Faraday cage initially increased as expected but oscillated once the frequency shift stabilized. (b) Frequency response with Faraday cage still portrayed oscillatory behavior.

4. CONCLUSION

An affinity-based biosensor capable of IgG detection was demonstrated toward the development of a versatile biosensor platform with the potential for next-generation applications. The QCM biosensor system portrayed response linearity across 10 μg/mL to 1 mg/mL of analyte, and the construction of the recognition element showed promise for effective capture of IgG in surface characterization and binding studies. Stability of the biosensor was the biggest concern, with the inversion of the frequency response and oscillatory response behavior proving problematic. However, certain concessions in performance had to be made for a custom benchtop biosensor with susceptibility to electromagnetic interference and other environmental factors. The addition of temperature control could potentially have solved the issue of abnormal response behavior, but that would have drastically increased the complexity of the biosensor system. Although the instrumentation used to validate the QCM was complex and expensive on its own, the core makeup of the biosensor (QCM, PCB, microfluidic chamber) only costed several hundreds of dollars which is key for accessible management of health across the globe, especially when enabled with biosensor regeneration and arrayed detection.

4.1 FUTURE DIRECTION

The experiments in this body of work pertained to the creation of a QCM biosensor system and conduction of baseline studies to characterize performance. More work needs to be done to characterize the overall robustness of the system, such as operation in complex media to show selectivity for IgG when surrounded by contaminants and competitor species. This would provide a more accurate picture of biosensor performance regarding practical utility. However, prior to adding complexity within the liquid sample, understanding the correlation between analyte concentration and binding rate would be key for solidifying biosensor specifications. More

experiments utilizing one concentration of IgG per QCM biosensor would be useful for understanding reproducibility. One of the biggest unknowns of the biosensor was the spatial density of the recognition element on the QCM surface, which has a drastic impact on sensitivity, frequency response behavior, and extending the dynamic range of detection. Varying incubation times of functionalization steps during biosensor preparation could have an impact on binding efficacy, but a more quantitative analysis of the spatial density or uniform "packing" of the recognition element on the surface would be invaluable. Additionally, implementing better temperature control and electromagnetic shielding would be sensible steps to ensure that the frequency response behavior is mostly influenced by surface phenomena and not as much affected by or subjected to external conditions.

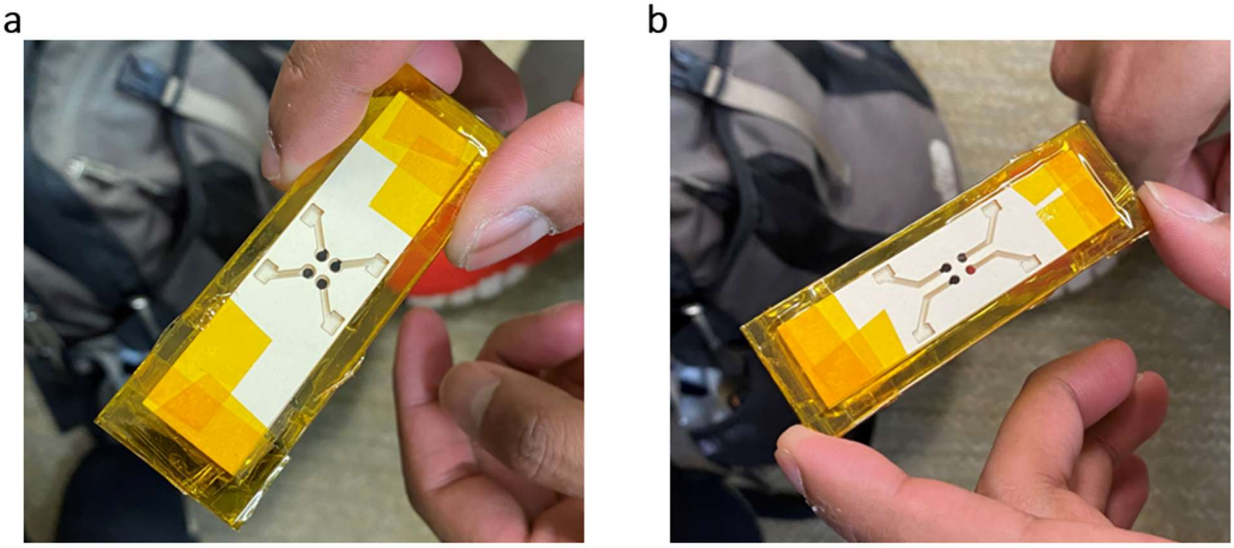

Figure 41. Arrayed QCM with thermal evaporator deposition mask on rectangular quartz. (a) Top of the arrayed QCM with four detection regions. (b) Back of the arrayed QCM with overlapping electrodes. Courtesy of Dr. Srivatsan Ramesh, BioPep Lab.

The development of a QCM for arrayed detection and biosensor regeneration techniques are also vital next steps. Efforts down this path began by fabricating four QCM sensors on a rectangular quartz crystal as shown in Figure 41. Some essence of the resonant frequency peaks

was observed using the VNA, but they did not correspond to the thickness of the crystal. For the time being, commercial QCM crystals produced through polished manufacturing processes are the best choice for understanding surface phenomena as to not add more variables to the system. Arrayed QCM setups would follow the same initial testing of the single QCM biosensor, highlighting the differences in operation between liquid and air, and using various mixtures of glycerol in water to assess frequency response behavior. Biosensor regeneration was explored using sodium phosphate in NaCl (Figure 42) and Glycine-HCl as chemical regeneration solutions, as well as maintaining the amplitude of the QCM at higher magnitudes for extended periods of time.

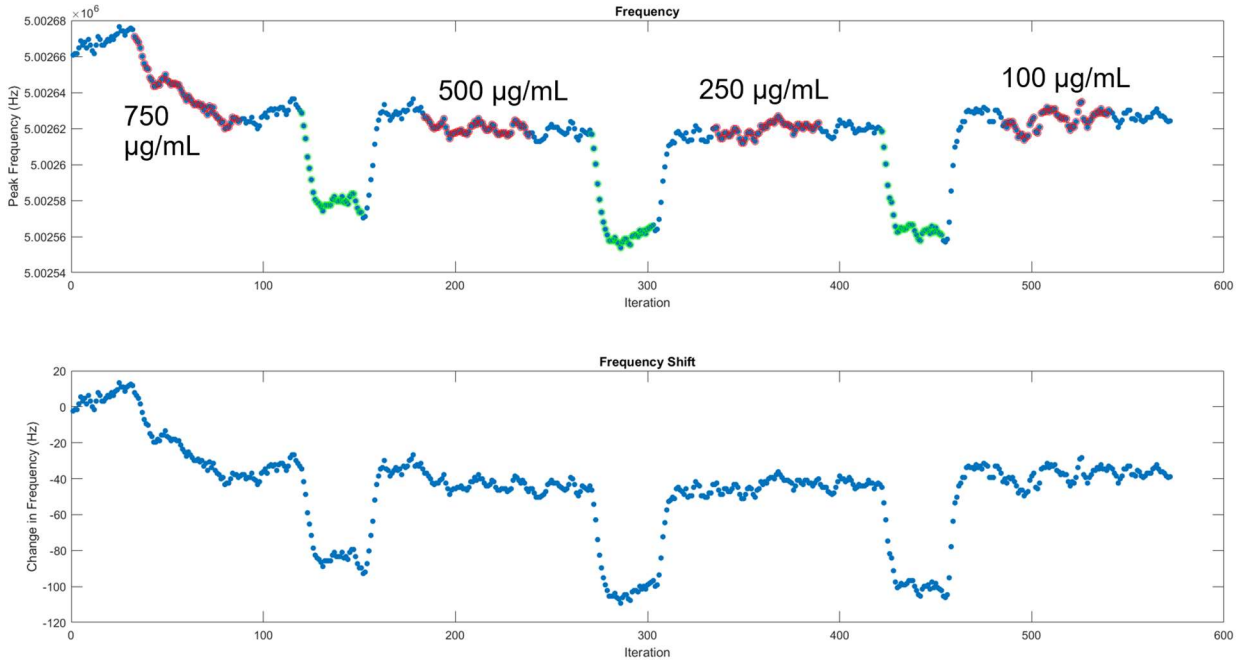

Figure 42. Sodium phosphate in NaCl biosensor regeneration experiment. First introduction of IgG (red) with 750 µg/mL followed the expected frequency response behavior. With the introduction of regeneration solution (green), the frequency drastically decreased but increased again with the reintroduction of PBS. Here, this particular regeneration solution did not work because the frequency responses remained at the initial saturation limit from the first concentration. Each iteration is 1 minute.

Overall, the question of signal stability remained, so more work should be done to address abnormal frequency responses and assess the QCM performance using standard IgG experiments. Ideally, once stable operation of the QCM biosensor system can be understood and soundly executed, the exploration of biosensor regeneration would start by replicating examples in the literature that utilize chemical regeneration schemes with acids or detergents. These studies would serve as the baseline comparison for regeneration using other methods such as mechanical or kinetic regeneration through vibration. The QCM biosensor system developed in this body of work is prime for multi-analyte arrayed detection and biosensor regeneration investigations, and has immense potential to be adapted toward a plethora of biomedical applications such as the routine, accessible, and comprehensive management of health conditions.

REFERENCES

1. Lovly, C., Berger, M., Vnencak-Jones, C., *Circulating Tumor DNA.* My Cancer Genome, 2016.

2. Pruthi, S., *Biopsy: Types of biopsy procedures used to diagnose cancer.* Mayo Foundation for Medical Education and Research (MFMER), 2021.

3. Alix-Panabières, C., Pantel, K., *Liquid biopsy: from discovery to clinical implementation.* Molecular Oncology, 2021. **15**(6): p. 1617-1621.

4. Singh, S., Podder, P., Russo, M., Henry, C., Cinti, S., *Tailored point-of-care biosensors for liquid biopsy in the field of oncology.* Lab on a Chip, 2023. **23**: p. 44-61.

5. Bhalla, N., Jolly, P., Formisano, N., Estrela, P., *Introduction to biosensors.* Essays in Biochemistry, 2016. **60**(1): p. 1-8.

6. Bag, S., Mandal, D., *Overview of Biosensors and Its Application in Health Care.* Next Generation Smart Nano-Bio-Devices, 2022: p. 29-60.

7. Wang, W., Mai, Z., Chen, Y. et al., *A label-free fiber optic SPR biosensor for specific detection of C-reactive protein.* Scientific Reports, 2017. **7**.

8. Baek, I., Byun, S., Lee, B. et al., *Attogram mass sensing based on silicon microbeam resonators.* Scientific Reports, 2017. **7**.

9. Gupta, A., Animesh, S., Singh, A., *An Overview of Immunosensors and Their Application.* Biomaterials-Based Sensors, 2023: p. 245-290.

10. Wisniewski, N., Reichert, M., *Methods for reducing biosensor membrane biofouling.* Colloids and Surfaces B: Biointerfaces, 2000. **18**(3-4): p. 197-219.

11. Al-Janabi, S., Al-Janabi, I., Al-Janabi, N., *Chapter 10 - Analysis the structural, electronic and effect of light on PIN photodiode achievement through SILVACO software: a case study.* Data Science for Genomics, 2023: p. 165-178.

12. *Signal-to-Noise Ratio as a Quantitative Measure for Optical Biosensors.* Maxim Integrated Products, Inc., 2014.

13. Thiviyanathan, V., Gorenstein, D., *Aptamers and the next generation of diagnostic reagents.* Proteomics - Clinical Applications, 2012. **6**(11-12): p. 563-573.

14. Dhar, P., Samarasinghe, R., Shigdar, S., *Antibodies, Nanobodies, or Aptamers—Which Is Best for Deciphering the Proteomes of Non-Model Species?* International Journal of Molecular Sciences, 2020. **21**(7).

15. Scheller, F., Yarman, A., Bachmann, T., et al., *Future of biosensors: a personal view.* Advances in Biochemical Engineering/Biotechnology, 2014. **140**: p. 1-28.

16. Goode, J., Rushworth, J., Millner, P., *Biosensor Regeneration: A Review of Common Techniques and Outcomes.* Langmuir, 2015. **31**(23): p. 6267-6276.

17. Liu, J., Jasim, I., Shen, Z., et al., *A microfluidic based biosensor for rapid detection of Salmonella in food products.* PLOS ONE, 2019. **14**(5).

18. Pauliukaite, R., Voitechovič, E., *Multisensor Systems and Arrays for Medical Applications Employing Naturally-Occurring Compounds and Materials.* Sensors, 2020. **20**(12).

19. Eddin, F., Fen, Y., *The Principle of Nanomaterials Based Surface Plasmon Resonance Biosensors and Its Potential for Dopamine Detection.* Molecules, 2020. **25**(12).

20. Zhou, Y., Chiu, C., Liang, H., *Interfacial Structures and Properties of Organic Materials for Biosensors: An Overview.* Sensors, 2012. **12**(11): p. 15036-15062.

21. Febriansyah, A., Nuryadi, R., Hartanto, D., *Measurement and Simulation Techniques for Piezoresistive Microcantilever Biosensor Applications.* TELKOMNIKA, 2012. **10**(4): p. 725-732.

22. Bakhtiar, R., *Surface Plasmon Resonance Spectroscopy: A Versatile Technique in a Biochemist's Toolbox.* Journal of Chemical Education, 2013. **90**(2): p. 203-209.

23. Nguyen, H., Park, J., Kang, S., Kim, M., *Surface Plasmon Resonance: A Versatile Technique for Biosensor Applications.* Sensors (Basel), 2015. **15**(5): p. 10481-10510.

24. Mandal, D., Banerjee, S., *Surface Acoustic Wave (SAW) Sensors: Physics, Materials, and Applications.* Sensors, 2022. **22**(3).

25. Länge, K., Rapp, B., Rapp, M., *Surface acoustic wave biosensors: a review.* Analytical and Bioanalytical Chemistry, 2008. **391**: p. 1509-1519.

26. Fogel, R., Limson, J., Seshia, A., *Acoustic biosensors.* Essays in Biochemistry, 2016. **60**(1): p. 101-110.

27. Leïchlé, T., Nicu, L., Alava, T., *MEMS Biosensors and COVID-19: Missed Opportunity.* ACS Sensors, 2020. **5**(11): p. 3297-3305.

28. Mouro, J., Pinto, R., Paoletti, P., Tiribilli, B., *Microcantilever: Dynamical Response for Mass Sensing and Fluid Characterization.* Sensors (Basel), 2021. **21**(1).

29. Lu, H., Zada, S., Yang, L., Dong, H., *Microneedle-Based Device for Biological Analysis.* Frontiers in Bioengineering and Biotechnology, 2022. **10**.

30. Miranda, B., Battisti, M., Martino, S., et al., *Hollow Microneedle-based Plasmonic Sensor for on Patch Detection of Molecules in Dermal Interstitial Fluid.* Advanced Materials Technologies, 2023. **8**(14).

31. Yuwono, A., Lammers, P., *Performance Test of a Sensor Array - Based Odor Detection Instrument.* Agricultural Engineering International: the CIGR Journal of Scientific Research and Development, 2004.

32. Sauerbrey, G., *Verwendung von Schwingquarzen zur Wägung dünner Schichten und zur Mikrowägung.* Zeitschrift für Physik, 1959. **155**: p. 206-222.

33. *Quartz Crystal Microbalance (QCM).* Nanoscience Instruments.

34. Warner, A., Stockbridge, C., *Quartz Resonators; Reduction of Transient Frequency Excursion Due to Temperature Change.* Journal of Applied Physics, 1963. **34**(2): p. 437-438.

35. Barnes, C., *Some new concepts on factors influencing the operational frequency of liquid-immersed quartz microbalances.* 1992. **30**(3): p. 197-202.

36. Kanazawa, K., Gordon, J., *Frequency of a quartz microbalance in contact with liquid.* Analytical Chemistry, 1985. **57**(8): p. 1770-1771.

37. Mauro, M., *openQCM test of quartz crystal in contact with liquid.* openQCM, Novaetech S.r.l, 2016.

38. Castro, P., et al., *Apparent negative mass in QCM sensors due to punctual rigid loading.* IOP Conference Series: Materials Science and Engineering, 2012. **42**.

39. Liebherr, R., *Development of a Magnetically Enhanced Quartz Crystal Microbalance.* University of Nevada, Reno., 2011.

40. Edvardsson, M., *4 steps to prevent temperature related problems in QCM measurements.* Surface Science Blog, Biolin Scientific, 2023.

41. Wang, P., Ling, M., Li, M., *Design and Analysis of Quartz Crystal Microbalance with a New Ring-Shaped Interdigital Electrode.* Sensors, 2022. **22**(19).

42. Afzal, A., Mujahid, A., Schirhagl, R., et al., *Gravimetric Viral Diagnostics: QCM Based Biosensors for Early Detection of Viruses.* Chemosensors, 2017. **5**(1).

43. Zainuddin, A., Nordin, A., Rahim, R., et al., *Verification of Quartz Crystal Microbalance Array using Vector Network Analyzer and OpenQCM.* Indonesian Journal of Electrical Engineering and Computer Science, 2018. **10**(1): p. 84-93.

44. Joseph, A., Emadi, A., *A High Frequency Dual Inverted Mesa QCM Sensor Array With Concentric Electrodes.* IEEE Access, 2020. **8**.

45. *5 MHz quartz crystal sensors - 10 pieces.* openQCM, Novaetech S.r.l.

46. *10 MHZ QUARTZ SENSORS BOX FOR LIQUID BIOSENSING- 10 PIECES.* openQCM, Novaetech S.r.l.

47. Sota, H., Yoshimine, H., Whittier, R., *A Versatile Planar QCM-Based Sensor Design for Nonlabeling Biomolecule Detection.* Analytical Chemistry, 2002. **74**(15): p. 3592-3598.

48. Robinson, J., *What Is an Immunoglobulin Test?* WebMD, 2023.

49. Hirsch, L., *Blood Test: Immunoglobulins (IgA, IgG, IgM).* Nemours Children's Health, 2020.

50. Janeway, C., Travers, P., Walport, M., et al., *The structure of a typical antibody molecule.* Immunobiology: The Immune System in Health and Disease. 5th edition., 2001.

51. Kiernan, C., Knuth, C., Farrell, E., *Chapter 6 - Endochondral Ossification: Recapitulating Bone Development for Bone Defect Repair.* Developmental Biology and Musculoskeletal Tissue Engineering - Principles and Applications, 2018: p. 125-148.

52. Suzuki, M., Kato, C., Kato, A., *Therapeutic antibodies: their mechanisms of action and the pathological findings they induce in toxicity studies.* Journal of Toxicologic Pathology, 2015. **28**(3): p. 133-139.

53. Chiu, M., Goulet, D., Teplyakov, A., Gilliland, G., *Antibody Structure and Function: The Basis for Engineering Therapeutics.* Antibodies, 2019. **8**(4).

54. Malik, B., Ghatol, A., *Understanding How Monoclonal Antibodies Work.* StatPearls, 2023.

55. *Recombinant Monoclonal Antibodies.* Bio-Techne.

56. *Monoclonal Antibodies and Their Side Effects.* American Cancer Society, 2022.

57. Lagaditis, P., *Piranha Solution.* Occupational Health, Safety and Environment - Chemical Safety – Special Hazards, 2022.

58. Wasilewski, T., Szulczyński, B., Dobrzyniewski, D., et al., *Development and Assessment of Regeneration Methods for Peptide-Based QCM Biosensors in VOCs Analysis Applications.* Biosensors (Basel), 2022. **12**(5).

59. Whitesides, G., Mrksich, M., *Using Self-Assembled Monolayers to Understand the Interactions of Man-made Surfaces with Proteins and Cells.* Annual Review of Biophysics and Biomolecular Structure, 1996. **25**: p. 55-78.

60. Brothers, M., Moore, D., Lawrence, M., et al., *Impact of Self-Assembled Monolayer Design and Electrochemical Factors on Impedance-Based Biosensing.* Sensors (Basel), 2020. **20**(8).

61. *Chemical Sketch Tool.* Powered by ChemAxon. Research Collaboratory for Structural Bioinformatics Protein Data Bank.

62. Naik, A., Menegatti, S., Gurgel, P., Carbonell, R., *Performance of hexamer peptide ligands for affinity purification of immunoglobulin G from commercial cell culture media.* Journal of Chromatography A, 2011. **1218**(13): p. 1691-1700.

63. Yang, H., Gurgel, P., Carbonell, R., *Purification of human immunoglobulin G via Fc-specific small peptide ligand affinity chromatography.* Journal of Chromatography A, 2009. **1216**(6): p. 910-918.

64. Yang, H., Gurgel, P., Williams, K., et al., *Binding site on human immunoglobulin G for the affinity ligand HWRGWV.* Journal of Molecular Recognition, 2010. **23**(3): p. 271-282.

65. *PepDraw.* The Wimley Lab, Tulane University, 2011.

66. Shen, F., *Affinity Interaction between Hexamer Peptide Ligand HWRGWV and Immunoglobulin G Studied by Quartz Crystal Microbalance and Surface Plasmon Resonance.* North Carolina State University, 2010.

67. Shen, F., Rojas, O., Genzer, J., Gurgel, P., Carbonell, R., *Affinity interactions of human immunoglobulin G with short peptides: role of ligand spacer on binding, kinetics, and mass transfer.* Analytical and Bioanalytical Chemistry, 2015. **408**(2016): p. 1829-1841.

68. Chu, W., Prodromou, R., Day, K., et al., *Peptides and pseudopeptide ligands: a powerful toolbox for the affinity purification of current and next-generation biotherapeutics.* Journal of Chromatography A, 2021. **1635**.

69. Rodenhausen, B., *How to analyze combined QCM-D and ellipsometry data.* White Paper, Biolin Scientific, 2018.

70. Plikusiene, I., Maciulis, V., Ramanavicius, A., Ramanaviciene, A., *Spectroscopic Ellipsometry and Quartz Crystal Microbalance with Dissipation for the Assessment of Polymer Layers and for the Application in Biosensing.* Polymers, 2022. **14**.

71. *Ellipsometry Measurements.* Tutorial, J.A. Woollam.

72. *Scientific Principles of PiFM and PiF-IR.* Photo-Induced Force Microscopy and Spectroscopy, Molecular Vista.

73. Johannsmann, D., Langhoff, A., Leppin, C., *Studying Soft Interfaces with Shear Waves: Principles and Applications of the Quartz Crystal Microbalance (QCM).* Sensors, 2021. **21**.

74. Burda, I., *Quartz Crystal Microbalance with Impedance Analysis Based on Virtual Instruments: Experimental Study.* Sensors (Basel), 2022. **22**(4).

75. Fort, A., Panzardi, E., Vignoli, V., et al., *An Adaptive Measurement System for the Simultaneous Evaluation of Frequency Shift and Series Resistance of QCM in Liquid.* Sensors (Basel), 2021. **21**(3).

76. Schneider, T., Frye-Mason, G., Martin, S., et al., *Chemically Selective Coated Quartz Crystal Microbalance (QCM) Array for Detection of Volatile Organic Chemicals.* Microsensor Research and Development Department, Sandia National Laboratories, 1998.

77. Seifried, B., Temelli, F., *Use and limitations of a quartz crystal microbalance to measure viscosity of carbon dioxide-expanded fish oil fatty acid ethyl esters.* The Journal of Supercritical Fluids, 2015. **101**: p. 104-109.

78. Johannsmann, D., Reviakine, I., Richter, R., *Dissipation in Films of Adsorbed Nanospheres Studied by Quartz Crystal Microbalance (QCM).* Analytical Chemistry, 2009. **81**(19): p. 8167-8176.

79. Michalzik, M., Wilke, R., Büttgenbach, S., *Miniaturized QCM-based flow system for immunosensor application in liquid.* Sensors and Actuators B: Chemical, 2005. **111-112**(11): p. 410-415.

80. Hieda, M., Garcia, R., Dixon, M., et al., *Ultrasensitive quartz crystal microbalance with porous gold electrodes.* Applied Physics Letters, 2004. **84**(4).

81. Cassiede, M., Daridon, J., Paillol, J., Pauly, J., *Impedance analysis for characterizing the influence of hydrostatic pressure on piezoelectric quartz crystal sensors.* Journal of Applied Physics, 2010. **108**.

82. Huang, P., Scace, G., Hodges, J., *Referencing Dilution-Based Trace Humidity Generators to Primary Humidity Standards.* National Institute of Standards and Technology, Gaithersburg, Maryland, USA.

83. Auge, J., Hauptmann, P., Hartmann, J., et al., *New design for QCM sensors in liquids.* Sensors and Actuators B: Chemical, 1995. **24**(1-3): p. 43-48.

84. Yoshimoto, M., Kurosawa, S., *Effect of Immersion Angle of a One-Face Sealed Quartz Crystal Microbalance in Liquid.* Analytical Chemistry, 2002. **74**: p. 4306-4309.

85. Nivens, D., Chambers, J., Anderson, T., White, D., *Long-term, on-line monitoring of microbial biofilms using a quartz crystal microbalance.* Analytical Chemistry, 1993. **65**(1): p. 65-69.

86. *Fluidic Configurations for QCM-I: Quartz Crystal Microbalance with Impedance Analysis.* Technical Note, MicroVacuum.

87. *Principles of Lock-in Detection.* Resources, Zurich Instruments, 2023.

88. *Faraday Cage: What Is It? How Does It Work?* Instrumentation, Gamry Instruments.

89. *Thickness Shear Mode Quartz Oscillator.* COMSOL, Application ID: 4707.

90. Esmeryan, K., McHale, G., Trabi, C., et al., *Manipulated wettability of a superhydrophobic quartz crystal microbalance through electrowetting.* Journal of Applied Physics D: Applied Physics, 2013. **46**(34).

91. White, C., Clinton, W., Weiss, R., Bryan, V., *Unexpected frequency behavior in QCM-D: When can frequency increase with increased adhered mass?* Soft Matter, 2018. **90**(6).

92. Sadman, K., Wiener, C., Vogt, B., et al., *Quantitative Rheometry of Thin Soft Materials Using the Quartz Crystal Microbalance with Dissipation.* Analytical Chemistry, 2018. **90**(6): p. 4079-4088.

APPENDICES

APPENDIX A – LABVIEW DIAGRAMS

The user-friendly front panel (Figure A1) displayed the input fields to initialize the system as well as plots for the scattering parameters, to visualize the peak and amplitude of the resonant frequency of the QCM. The back-end block diagram (Figure A2) was used to manipulate the front panel and run experiments by writing data to a file looped over a specified number of iterations.

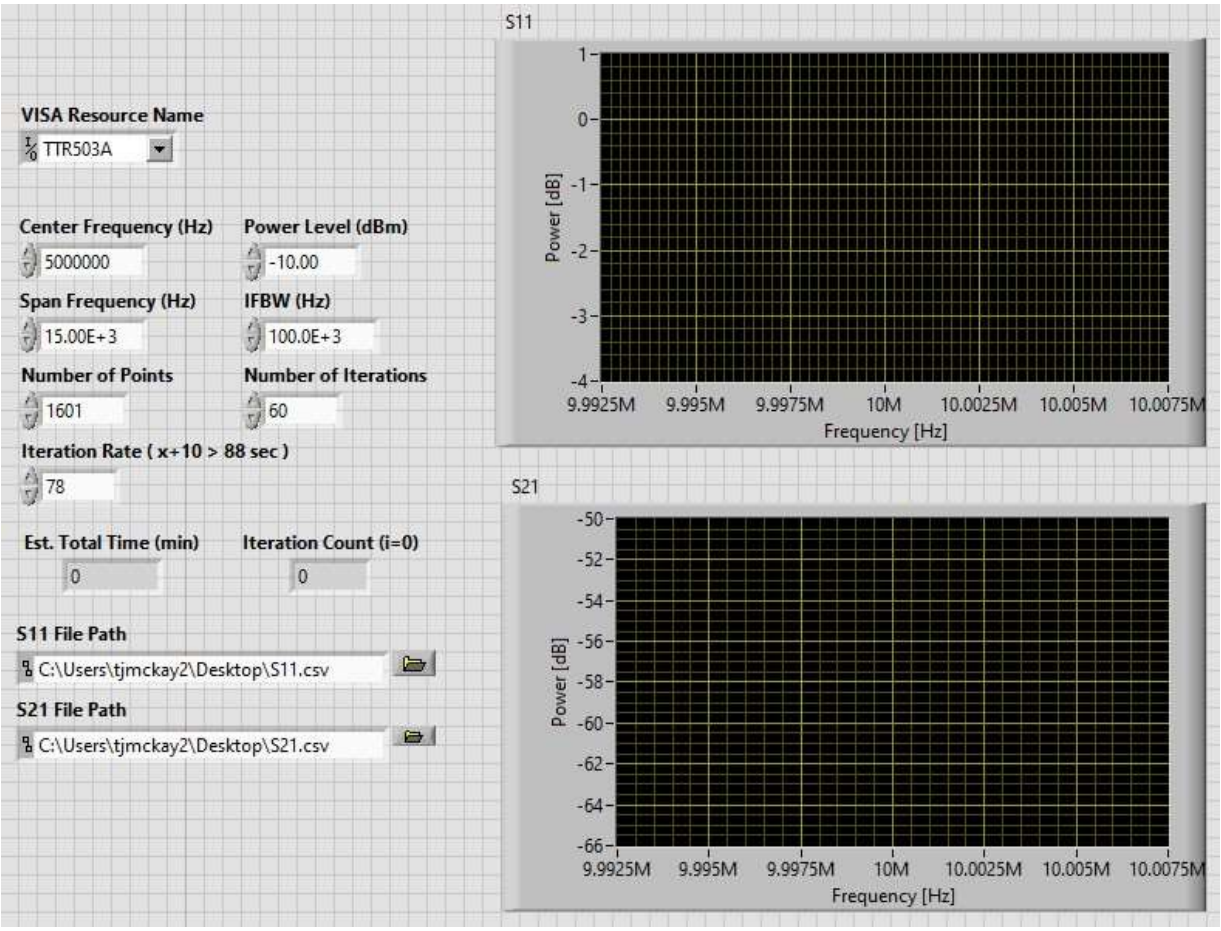

Figure A1. LabVIEW front panel.

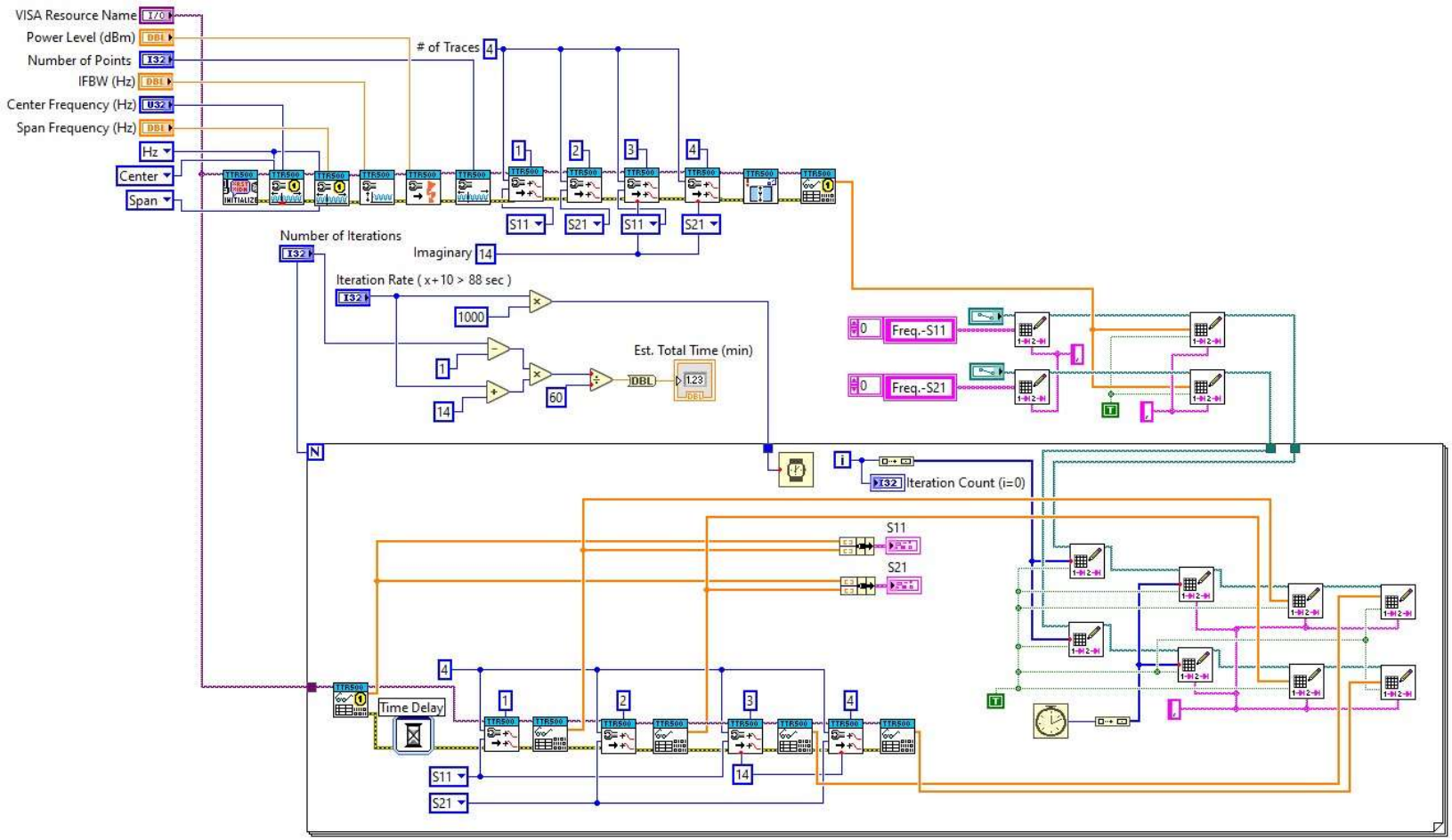

Figure A2. LabVIEW block diagram.

APPENDIX B – MATLAB CODE

The base code below was used to visualize the amplitude, amplitude shift, frequency, and frequency shift of the resonant frequency (peak) during QCM experiments to generate plots such as those found in Figure 30. This code was also modified to produce plots for other variations of experiments, such as consecutive concentrations of analyte and PBS baseline stability tests.

```
close all
clear all
clc

% import raw data files
data1 = xlsread(['1015_1.csv']); % initial PBS baseline
data2 = xlsread(['1015_2.csv']); % IgG / analyte sample
data3 = xlsread(['1015_3.csv']); % post PBS baseline


% concatenate raw data
data = [data1;data2;data3];

% extract relevant data from files
data = data(:,5:end);
frequency = data(8,:);
amplitude = data(15:29:end,:);

iteration_start = 1;

amplitude = amplitude(iteration_start:end,:);

m = size(amplitude,1) % number of data points

% iteration data
iteration = (1:1:m)

spi = 67 % how many "seconds per iteration"?
timetotal = spi*m % total time
time = 1:spi:timetotal % convert time matrix to seconds
time = time./60 % convert time matrix to minutes

% Amplitude (dB) analysis:

max_amp = max(amplitude,[],2); % min/max values from every iteration
max_amp_0 = max_amp(1); % set initial min / max value

amp_shift = max_amp - max_amp_0; % evaluate shift in amplitude values

% graph amplitude values
scatter(time,max_amp,8,'filled')
xlabel('time (min)')
ylabel('amplitude (V)')

% graph shift in amplitude values
figure
scatter(time,amp_shift,8,'filled')
```

```
xlabel('time (min)')
ylabel('amplitude shift (V)')

% Peak frequency (Hz) analysis:

% find frequency of peak values from every iteration
for i = 1:length(iteration)

    max_freq = find(amplitude(i,:) == max_amp(i));
    xvalue = max_freq(1);
    y = frequency(xvalue);
    R_matrix(i,1) = y;

end

f0 = R_matrix(1); % set initial peak frequency value
freq_shift = R_matrix - f0; % evaluate shift in peak freqency values

% graph peak frequency
figure
scatter(time,R_matrix,8,'filled')
xlabel('time (min)')
ylabel('peak frequency (Hz)')

% graph shift in peak frequency
figure
scatter(time,freq_shift,8,'filled')
xlabel('time (min)')
ylabel('frequency shift (Hz)')

hold on % to change color of analyte data points on plot

a = 38 % input number of initial PBS baseline points
b = 51 % input number of IgG / analyte data points
c = 44 % input number of post PBS baseline points

r1 = a; % number of PBS baseline points
r2 = r1 + b; % cumulative number of points up to IgG /anlayte sample
r3 = r2 + c; % cumulative number of points overall (total)

% change color of IgG / analyte sample data points to red
scatter(time(r1:r2),freq_shift(r1:r2),8,'r','filled')

hold off
```